Inorganic Chemistry

Article

pubs.acs.org/IC

Substitution Reactions in Dinuclear Ru-Hbpp Complexes: an Evaluation of Through-Space Interactions

Nora Planas,[†] Gemma Christian,[†] Stephan Roeser,[†] Elena Mas-Marzá,[†] Mohan-Rao Kollipara,[‡] Jordi Benet-Buchholz,[†] Feliu Maseras,*[,†,‡] and Antoni Llobet*[,†,‡]

[†]Institute of Chemical Research of Catalonia (ICIQ), Av. Països Catalans 16, E-43007 Tarragona, Spain

[‡]Departament de Química, Universitat Autònoma de Barcelona, Cerdanyola del Vallès, 08193 Barcelona, Spain

Supporting Information

ABSTRACT: The synthesis of new dinuclear complexes of the general formula *in,in*-{[Ru^{II}(trpy)(L)](μ-bpp)[Ru^{II}(trpy)(L′)]}$^{3+}$ [bpp$^-$ is the bis(2-pyridyl)-3,5-pyrazolate anionic ligand; trpy is the 2,2′:6′,2″-terpyridine neutral meridional ligand, and L and L′ are monodentate ligands; L = L′ = MeCN, **3a**$^{3+}$; L = L′ = 3,5-lutidine (Me_2-py), **3c**$^{3+}$; L = MeCN, L′ = pyridine (py), **4**$^{3+}$], have been prepared and thoroughly characterized. Further, the preparation and isolation of dinuclear complexes containing dinitrile bridging ligands of the general formula *in,in*-{[Ru^{II}(trpy)]$_2$(μ-bpp)(μ-L-L)}$^{3+}$ [μ-L-L = 1,4-dicyanobutane (adiponitrile, adip), **6a**$^{3+}$; 1,3-dicyanopropane (glutaronitrile, glut), **6b**$^{3+}$; 1,2-dicyanoethane (succinonitrile; succ), **6c**$^{3+}$] have also been carried out. In addition, a number of homologous dinuclear complexes previously described, containing the anionic bis(pyridyl)-indazolate (bid$^-$) tridentate meridional ligand in lieu of trpy, have also been prepared for comparative purposes. In the solid state, six complexes have been characterized by X-ray crystallography, and in solution, all of them have been spectroscopically characterized by NMR and UV−vis spectroscopy. In addition, their redox properties have also been investigated by means of cyclic voltammetry and differential pulse voltammetry and show the existence of two one-electron waves assigned to the formation of the II,III and III,III species. Dinitrile complexes **6a**$^{3+}$, **6b**$^{3+}$, and **6c**$^{3+}$ display a dynamic behavior involving their enantiomeric interconversion. The energy barrier for this interconversion can be controlled by the number of methylenic units between the dinitrile ligand. On the other hand, pyridyl complexes *in,in*-{[Ru^{II}(T)(py)]$_2$(μ-bpp)}$^{n+}$ (T = trpy, n = 3, **3b**$^{3+}$; T = bid$^-$, n = 1, **3b**′$^{+}$) and **3c**$^{3+}$ undergo two consecutive substitution reactions of their monodentate ligands by MeCN. The substitution kinetics have been monitored by ^{1}H NMR and UV−vis spectroscopy and follow first-order behavior with regard to the initial ruthenium complex. For the case of **3b**$^{3+}$, the first-order rate constant $k_1 = (2.9 \pm 0.3) \times 10^{-5}$ s^{-1}, whereas for the second substitution, the k obtained is $k_2 = (1.7 \pm 0.7) \times 10^{-6}$ s^{-1}, both measured at 313 K. Their energies of activation at 298 K are 114.7 and 144.3 kJ mol^{-1}, respectively. Density functional theory (DFT) calculations have been performed for two consecutive substitution reactions, giving insight into the nature of the intermediates. Furthermore, the energetics obtained by DFT calculations of the two consecutive substitution reactions agree with the experimental values obtained. The kinetic properties of the two consecutive substitution reactions are rationalized in terms of steric crowding and also in terms of through-space interactions.

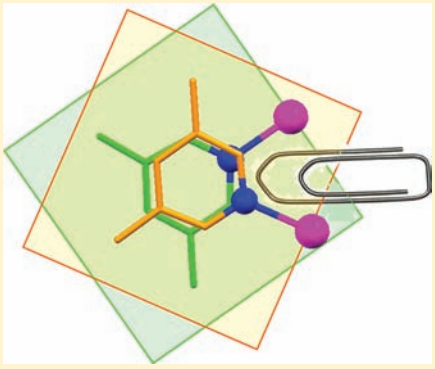

INTRODUCTION

Ruthenium complexes are of interest for a variety of applications including bioinorganic chemistry, photochemistry, photophysics, and catalysis.[1] In all of these cases, the kinetics and thermodynamics of ligand substitution is of paramount importance so that the complex can be used for the desired applications. For the particular case of catalysis, ruthenium complexes are generally designed with at least one labile Ru−L bond so that easy substitution by a particular substrate is possible, thus entering into a potential catalytic cycle for its subsequent transformation.[2] In some cases, such as hydrogenation[3] or hydroformylation[4] reactions, the substitution process constitutes the rate-determining step, and thus it is important to understand at the molecular level the factors that govern these processes. For instance, for complexes that interact with DNA, two main types of interactions can take place: $\pi-\pi$ stacking between the nucleobases and the aromatic rings of the ligands and direct coordination of the Ru metal to a potential coordination site of the DNA. For the latter, a sufficiently labile Ru−L bond is needed, further demonstrating the importance of substitution reactions.[5]

A recent example in water oxidation catalysis[6] involving the [Ru(Cl)(trpy)(bpy)]$^{2+}$ (bpy represents 2,2′-bipyridine and also its 4,4′-substituted analogues, and trpy is the 2,2′:6′,2″-terpyridine neutral meridional ligand) family of catalysts highlights the importance of understanding the substitution process. While an inert Ru−Cl bond leads the authors to

Received: October 13, 2011
Published: January 13, 2012

   dx.doi.org/10.1021/ic202225g | *Inorg. Chem.* 2012, 51, 1889−1901

propose a mechanism involving the expansion of the coordination,[7] leading to the metal center possessing seven-coordination, the presence of a labile Ru−Cl bond would implicate aqua substitution, forming a Ru−OH_2 bond and allowing maintenance of pseudooctahedral coordination for all of the intermediate species in the catalytic cycle.[8] For the case of the labile Ru−Cl bond, the relative rates for Ru−Cl substitution and for formation of the catalytic species Ru−OH_2 will dictate the feasibility of the whole catalytic process.

Within the same topic, equilibrium reactions involving solvent coordination such as MeCN for different oxidation states of the metal center, as well as exchange reactions, are key to understanding the catalytic cycle.[9]

$$\text{Ru-OH}_2 + \text{MeCN} \rightleftharpoons \text{Ru-MeCN} + \text{H}_2\text{O} \quad (1)$$

$$\text{Ru-OH}_2 + \text{H}_2\text{O}^* \rightleftharpoons \text{Ru-H}_2\text{O}^* + \text{H}_2\text{O} \quad (2)$$

In the particular case of *in*,in-RuHbpp complexes [*in*,*in*-{[(Ru(T)(L)]$_2$(μ-bpp)}$^{n+}$, where L = acetonitrile, pyridine, or 3,5-dimethylpyridine and T = trpy or bis(pyridyl)indazolate (bid$^-$); a drawing of the polydentate ligands is depicted in Scheme 1], an additional through-space interaction has to be

Scheme 1. Ligands Used in This Work

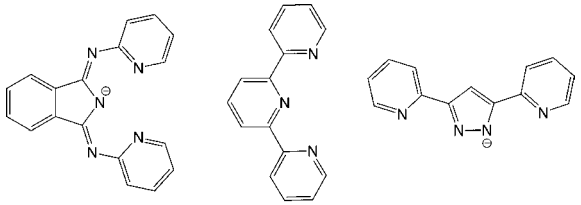

taken into consideration. This phenomenon is related to the through-space interaction between the monodentate ligands[10] and constitutes a specific case of the stereochemistry of ligand-bridged dinuclear coordination complexes. As exemplified in eq

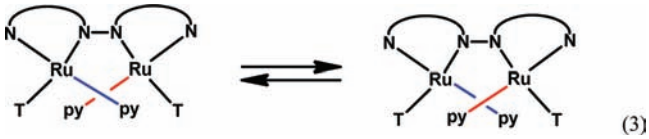

3 for complex **3b**$^{3+}$, in solution at room temperature, a very fast interconversion between the two atropisomeric enantiomers takes place.

Axial coordination of the trpy ligands is not shown for clarity, and the formula at the bottom excludes the trpy and bpp$^-$ [bis(2-pyridyl)-3,5-pyrazolate anionic ligand] ligands. The two isomers differ from one another in the relative position of the pyridyl ligands, whether they are situated above or below the equatorial plane. If temperature is maintained at room temperature or below, the equilibrium occurs without breaking any Ru−N bonds, as has been clearly demonstrated by NMR spectroscopy.[10] In the present work, we present new *in*,*in*-RuHbpp complexes containing bridging dinitrile ligands of the general formula {[Ru(trpy)]$_2$(μ-bpp)(μ-L-L)}$^{3+}$ [L-L = adiponitrile (adip), glutaronitrile (glut), or succinonitrile (succ)] and the study of the influence of the methylenic chain (linking the nitrile coordinating groups to the Ru centers) on the kinetics of enantiomeric interconversion indicated in eq 3.

Further, we also report that the *in*,*in*-RuHbpp-type complexes exposed to temperatures above room temperature undergo a Ru−N bond scission involving the monodentate ligand that is responsible for the substitution reactions. In order to describe the intimate details of the labile Ru−N bond scission, we have completed the synthesis of a large family of Ru-Hbpp complexes with the general formula {[Ru(T)(L)]$_2$-(μ-bpp)}$^{n+}$ (L = acetonitrile, pyridine, and 3,5-dimethylpyridine; T = trpy or bid$^-$) and have studied their substitution kinetics in conjunction with a complementary density functional theory (DFT) work.

EXPERIMENTAL SECTION

Materials. All reagents used in the present work were obtained from Aldrich Chemical Co. or Alfa Aesar and were used without further purification. Synthesis-grade organic solvents were obtained from SDS and were routinely degassed with argon. Methanol (MeOH) was distilled over MgI, ethanol was dried with a 3.5 Å molecular sieve, and acetonitrile, dichloromethane (DCM), hexane, and diethyl ether were used from the SPS. High-purity deionized water was obtained by passing distilled water through a nanopure Milli-Q water purification system.

The 3,5-bis(2-pyridyl)pyrazole (Hbpp) ligand,[11] [Ru^{III}Cl$_3$(Hbid)],[12] {[Ru(trpy)]$_2$(μ-bpp)(μ-AcO)}(PF$_6$)$_3$ [**2**(**PF$_6$**)$_3$],[13] {[Ru(bid)-(MeCN)]$_2$(μ-bpp)}(NO$_3$) [**3a′**(**NO$_3$**)], {[Ru(bid)(py)]$_2$(μ-bpp)}(Cl) [**3b′**(**Cl**)], and {[Ru(trpy)(py)]$_2$(μ-bpp)}(PF$_6$)$_3$ [**3b**(**PF$_6$**)$_3$] were prepared as described in the literature.[10]

All synthetic manipulations were routinely performed under an argon atmosphere using Schlenk and vacuum-line techniques. An NMR-labeling scheme is presented in the Supporting Information.

in,*in*-{[Ru^{II}(bid)(Cl)](μ-bpp)[Ru^{II}(bid)(MeOH)]} (**1′**). A solution of 0.290 g (0.5 mmol) of RuCl$_3$Hbid and 0.20 mL (1.5 mmol) of triethylamine in MeOH (10 mL) was stirred at room temperature, under an argon atmosphere and in the absence of light, for 30 min. Then, 0.056 g (0.25 mmol) of Hbpp, 0.014 g (0.25 mmol) of NaOMe, and 0.424 g (10 mmol) of LiCl were added to the initial mixture in 10 mL of MeOH. The resulting solution was heated at reflux for 2 h in the presence of a 200 W tungsten lamp, cooled to room temperature, and filtered off . The dark-green solid obtained was washed with diethyl ether and dried under vacuum. Yield: 80% (0.220 g). Anal. Calcd for $C_{50}H_{41}ClN_{14}ORu_2$: C, 55.02; H, 3.79; N, 17.96. Found: C, 54.80; H, 3.49; N, 17.57. ^{1}H NMR (400 MHz, DCM-d_2, 298 K, ppm): δ 1.89 (d, J_{L-O} = 4.58 Hz, 3H, H$_O$), 6.02 (t, J_{F-G} = J_{G-H} = 6.84 Hz, 2H, H$_G$), 6.15 (td, J_{f-g} = J_{g-h} = 6.33 Hz, J_{g-i} = 1.9 Hz, 2H, H$_g$), 6.53 (td, J_{C-D} = J_{E-D} = 5.91 Hz, J_{B-D} = 1.27 Hz, 1H, H$_D$), 6.58 (t, J_{c-d} = J_{d-e} = 5.91 Hz, 1H, H$_d$), 6.914 (q, J_{L-O} = 4.58 Hz, 1H, H$_L$), 7.05 (dd, J_{D-E} = 5.91 Hz, J_{C-E} = 1.47 Hz, 1H, H$_E$), 7.22 (dd, 1H, J_{d-e} = 5.91 Hz, J_{c-e} = 1.47 Hz, H$_e$), 7.38 (td, J_{C-D} = 5.91 Hz, J_{C-E} = 1.47 Hz, 1H, H$_C$), 7.42 (dd, J_{c-b} = 8.26 Hz, J_{c-d} = 5.91 Hz, 1H, H$_c$), 7.45 (dd, J_{H-I} = 6.84 Hz, J_{G-I} = 1.90 Hz, 2H, H$_I$), 7.51 (td, J_{g-h} = J_{h-i} = 6.33 Hz, J_{h-i} = 1.58 Hz, 2H, H$_i$), 7.54 (td, J_{G-H} = J_{H-I} = 6.84 Hz, J_{F-H} = 1.62 Hz, 2H, H$_H$), 7.58 (dd, J_{J-K} = 5.51 Hz, J_{J-K} = 3.13 Hz, 2H, H$_J$), 7.60 (t, J_{h-i} = J_{h-g} = 6.33 Hz, 2H, H$_h$), 7.65 (dd, J_{k-j} = 5.51 Hz, $J_{j-i'}$ = 3.13 Hz, 2H, H$_j$), 7.74 (dd, J_{B-C} = 8.26 Hz, J_{B-D} = 1.27 Hz, 1H, H$_B$), 7.76 (d, J_{b-c} = 8.26 Hz, J_{b-d} = 1.27 Hz, 1H, H$_b$), 7.80 (s, 1H, H$_A$), 8.15 (dd, J_{J-K} = 5.51 Hz, $J_{K-K'}$ = 3.13 Hz, 2H, H$_K$), 8.20 (d, J_{F-G} = 6.84 Hz, J_{F-H} = 1.62 Hz, 2H, H$_F$), 8.22 (dd, J_{k-j} = 5.51 Hz, $J_{k-k'}$ = 3.13 Hz, 2H, H$_k$), 8.30 (dd, J_{f-g} = 6.33 Hz, J_{f-h} = 1.58 Hz, 2H, H$_f$). UV−vis (CH_2Cl_2) [λ_{max}, nm (ε, M^{-1} cm^{-1})]: 271 (34 332), 279 (33 628), 303 (31 124), 368 (27 104), 424 (10 491), 609 (3516). $E_{1/2}$ (CH_2Cl_2, V vs SSCE): 0.204, 0.611.

in,*in*-{[Ru^{II}(trpy)(MeCN)]$_2$(μ-bpp)}(PF$_6$)$_3$ [**3a**(**PF$_6$**)$_3$]. A 100 mg (0.08 mmol) sample of complex *in*,*in*-{[Ru(trpy)]$_2$(μ-bpp)(μ-AcO)}(PF$_6$)$_3$ (0.08 mmol) was dissolved in 50 mL of MeCN/water (3:1), followed by the addition of 2 mL of a triflic acid aqueous solution (pH = 1). The mixture was heated at reflux for 6 h. Upon cooling to room temperature, the unreacted starting material was filtered and 1 mL of a

dx.doi.org/10.1021/ic202225g | Inorg. Chem. 2012, 51, 1889−1901

saturated aqueous solution of KPF_6 was added to the solution. After partial evaporation of the solvent in a rotary evaporator, a brown solid precipitated. Recrystallization from acetonitrile/ether yielded small dark-brown crystals. Yield: 70% (0.079 g). Anal. Calcd for $C_{47}H_{37}F_{18}N_{12}P_3Ru_2$: C, 40.12; H, 2.65; N, 11.95. Found: C, 40.37; H, 2.22; N, 11.75. ^{1}H NMR (400 MHz, acetone-d_6, 298 K, ppm): δ 1.43 (s, 6H, H_O), 7.02 (t, $J_{C-D} = J_{E-D} = 7.74$ Hz, 2H, H_D), 7.46 (d, $J_{D-E} = 7.74$ Hz, 2H, H_E), 7.56 (t, $J_{G-H} = J_{F-G} = 8.08$ Hz, 4H, H_G), 7.89 (t, $J_{B-C} = J_{C-D} = 7.74$ Hz, 2H, H_C), 8.15 (t, $J_{H-I} = J_{H-G} = 8.08$ Hz, 4H, H_H), 8.20 (d, $J_{B-C} = 7.74$ Hz, 2H, H_B), 8.39 (t, $J_{J-K} = 8.33$ Hz, 2H, H_K), 8.47 (s, 1H, H_A), 8.68 (d, $J_{H-I} = 8.08$ Hz, 4H, H_I), 8.80 (d, $J_{J-K} = 8.33$ Hz, 4H, H_J). ^{1}H NMR (400 MHz, MeCN-d_3, 240 K, ppm): δ 1.02 (s, 6H, H_O), 6.84 (t, $J_{C-D} = J_{E-D} = 7.74$ Hz, 2H, H_D), 7.13 (d, $J_{D-E} = 7.74$ Hz, 2H, H_E), 7.18 (t, $J_{G-H} = J_{F-G} = 8.08$ Hz, 2H, H_G), 7.43 (t, $J_{g-h} = J_{f-g} = 8.08$ Hz, 2H, H_g), 7.47 (d, $J_{f-g} = 8.00$ Hz, 2H, H_f), 7.74 (t, $J_{B-C} = J_{C-D} = 7.74$ Hz, 2H, H_C), 7.96 (d, $J_{B-C} = 7.74$ Hz, 2H, H_B), 8.00 (t, $J_{h-i} = J_{h-g} = 8.08$ Hz, 2H, H_h), 8.15 (s, 1H, H_A), 8.23 (t, $J_{J-K} = 8.33$ Hz, 2H, H_K), 8.35 (d, $J_{h-i} = 8.08$ Hz, 2H, H_i), 8.38 (d, $J_{F-G} = 8.00$ Hz, 2H, H_F), 8.43 (d, $J_{H-I} = 8.08$ Hz, 2H, H_I), 8.47 (d, $J_{J-K} = 8.33$ Hz, 2H, H_J), 8.43 (d, $J_{H-I} = 8.08$ Hz, 2H, H_I), 8.56 (d, $J_{j-k} = 8.33$ Hz, 2H, H_j). UV−vis (CH_2Cl_2) [λ_{max}, nm (ε, M^{-1} cm^{-1})]: 272 (59 626), 311 (70 425), 359 (26 803), 444 (13 238), 476 (11 874), 541 (3154). $E_{1/2}$ (CH_2Cl_2, V vs SSCE): 1.084, 1.392. MALDI(+)-MS (MeOH): 558.6 ([M − PF_6 − PF_6]$^{2+}$).

*in,in-{[Ru^{II}(trpy)(lut)]$_2$(μ-bpp)}(ClO$_4$)$_3$·CHCl$_3$ [**3c(ClO$_4$)$_3$·CHCl$_3$**].* A 50 mg sample of complex *in,in*-{[Ru(trpy)]$_2$(μ-bpp)(μ-AcO)}$(PF_6)_3$ (0.035 mmol) was dissolved in 40 mL of acetone/water (3:1), followed by the addition of 2 mL of a triflic acid aqueous solution (pH = 1). After the addition of 0.15 mL of 3,5-dimethylpyridine (4 mmol), the mixture was heated under reflux for 6 h. Upon cooling to room temperature, the unreacted starting material was filtered and 1 mL of a 1 M aqueous solution of $NaClO_4$ was added to the solution. After evaporation of the acetone in a rotary evaporator, a brown-black solid was obtained and recrystallized from chloroform/ether, yielding small dark-brown crystals. Yield: 90% (0.048 g). Anal. Calcd for $C_{58}H_{50}Cl_6N_{12}O_{12}Ru_2$: C, 45.77; H, 3.31; N, 11.04. Found: C, 45.65; H, 3.03; N, 10.90. ^{1}H NMR (400 MHz, acetone-d_6, 188 K, ppm): δ 1.24 (s, 6H, $H_{O'}$), 1.53 (s, 6H, H_O), 6.48 (s, 2H, H_L), 7.00 (t, $J_{E-D} = J_{CD} = 5.94$ Hz, 2H, H_D), 7.03 (s, 2H, $H_{L'}$), 7.41 (d, $J_{E-D} = 5.94$ Hz, 2H, H_E), 7.91 (t, $J_{F'-G'} = J_{H'-G'} = 4.90$ Hz, 2H, $H_{G'}$), 7.93 (t, $J_{F-G} = J_{H-G} = 5.26$ Hz, 2H, H_G), 7.95 (t, $J_{B-C} = J_{C-D} = 5.94$ Hz, 2H, H_C), 7.97 (s, 2H, H_N), 8.16 (t, $J_{H-I'} = J_{H'-G'} = 4.90$ Hz, 2H, $H_{H'}$), 8.28 (t, $J_{K-J} = J_{K-J'} = 8.35$ Hz, 2H, H_K), 8.33 (t, $J_{H-I} = J_{H-G} = 5.26$ Hz, 2H, H_H), 8.38 (d, $J_{B-C} = 5.94$ Hz, 2H, H_B), 8.46 (d, $J_{H'-I'} = 4.90$ Hz, 2H, $H_{I'}$), 8.54 (d, $J_{J'-K} = 8.35$ Hz, 2H, $H_{J'}$), 8.66 (d, $J_{F'-G'} = 4.90$ Hz, 2H, $H_{F'}$), 8.94 (d, $J_{H-I} = 5.26$ Hz, 2H, H_I), 8.95 (s, 1H, H_A), 8.97 (d, $J_{J-K} = 8.35$ Hz, 2H, H_J), 9.21 (d, $J_{F-G} = 5.26$ Hz, 2H, H_F). UV−vis (CH_2Cl_2) [λ_{max}, nm (ε, M^{-1} cm^{-1})]: 275 (54 000), 317 (62 450), 361 (25 704), 470 (9412), 502 (10 059), 566 (2439), 660 (1009). $E_{1/2}$ (CH_2Cl_2, V vs SSCE): 1.064, 1.332. MALDI(+)-MS (DCM): 1198.2 ([M − $CHCl_3$ − ClO_4 − lut]$^+$), 663 ([M − $CHCl_3$ − ClO_4 + Na]$^{2+}$).

*in,in-{[Ru^{II}(trpy)(py)](μ-bpp)[Ru^{II}(trpy)(MeCN)]}(PF$_6$)$_3$·CH$_2$Cl$_2$ [**4-(PF$_6$)$_3$·CH$_2$Cl$_2$**].* A 50 mg (0.035 mmol) sample of complex **3b**$(PF_6)_3$ was dissolved in 25 mL of MeCN. The mixture was heated at 70 °C for 3 h and quickly cooled with an ice bath. After fast complete evaporation of the solvent with a rotary evaporator, the brown product was redissolved in 5 mL of acetone, and 1 mL of a saturated aqueous solution of KPF_6 was added, followed by the addition of 5 mL of water. After partial evaporation of the acetone in a rotary evaporator, a brown solid precipitated. The dark,brown solid was filtered and rinsed with diethyl ether. Recrystallization from acetone/ether yielded small dark-brown crystals. Yield: 78% (0.039 g). Anal. Calcd for $C_{50}H_{39}F_{18}N_{12}P_3Ru_2$: C, 41.88; H, 2.97; N, 11.59. Found: C, 41.77; H, 2.72; N, 11.63. ^{1}H NMR (400 MHz, CD_3CN, 298 K, ppm): δ 1.27 (s, 3H, H_O), 6.70 (t, $J_{M-L} = J_{M-N} = 6.96$ Hz, 2H, H_M), 7.03 (t, $J_{D-E} = J_{D-C} = 7.23$ Hz, 1H, H_D), 7.04 (t, $J_{d-e} = J_{d-c} = 7.23$ Hz, 1H, H_d), 7.35 (d, $J_{e-d} = 7.23$ Hz, 1H, H_e), 7.43 (t, $J_{G-F} = J_{G-H} = 6.80$ Hz, 2H, H_G), 7.44 (t, $J_{N-M} = J_{N-M'} = 6.96$ Hz, 1H, H_N), 7.52 (d, $J_{E-D} = 6.96$ Hz, 1H, H_E), 7.73 (t, $J_{g-f} = J_{g-h} = 6.82$ Hz, 2H, H_g), 7.89 (t, $J_{c-d} = J_{c-b} = 7.23$ Hz, 1H, H_c), 7.96 (t, $J_{C-D} = J_{C-B} = 7.23$ Hz, 1H, H_C), 8.11 (t, $J_{H-I} = J_{H-G} = 6.80$ Hz, 2H, H_H) 8.20 (t, $J_{h-i} = J_{h-g} = 6.80$ Hz, 2H, H_h), 8.24 (d, $J_{b-c} = 7.23$ Hz, 1H, H_b), 8.26 (d, $J_{B-C} = 8.30$ Hz, 1H, H_B), 7.30 (t, $J_{k-j} = 8.10$ Hz, 1H, H_k), 8.33 (t, $J_{K-I} = 8.10$ Hz, 1H, H_K), 8.37 (d, $J_{f-g} = 8.10$ Hz, 2H, H_f), 8.46 (d, $J_{M-L} = 6.96$ Hz, 2H, H_L), 8.60 (d, $J_{F-G} = 6.82$ Hz, 2H, H_F), 8.60 (s, 1H, H_A), 8.68 (d, $J_{I-H} = 6.80$ Hz, 2H, H_I), 8.70 (d, $J_{i-h} = 6.80$ Hz, 2H, H_i), 8.75 (d, $J_{j-k} = 8.10$ Hz, 2H, H_j), 8.84 (d, $J_{J-K} = 8.10$ Hz, 2H, H_J). UV−vis (MeCN) [λ_{max}, nm (ε, M^{-1} cm^{-1})]: 271 (55 806), 312 (66 667), 356 (24 028), 440 (9127), 469 (11 727), 495 (8533), 574 (1856). $E_{1/2}$ (CH_2Cl_2, V vs SSCE): 1.086, 1.340. MALDI(+)-MS (MeOH): 1301.4 ([M − PF_6]$^+$).

*in,in-{[Ru^{II}(trpy)]$_2$(μ-bpp)(μ-adip)}(PF$_6$)$_3$ [**6a(PF$_6$)$_3$**].* A total of 40 mg (0.032 mmol) of complex *in,in*-{[Ru(trpy)]$_2$(μ-bpp)(μ-AcO)}-$(PF_6)_3$ was dissolved in 80 mL of acetone/water (3:1), followed by the addition of 2 mL of triflic acid aqueous solution (pH = 1). After the addition of 0.03 mL (0.3 mmol) of 1,4-dicyanobutane (adiponitrile, adip), the mixture was heated under reflux for 3 h. Upon cooling to room temperature, the unreacted starting material was filtered and 1 mL of a saturated aqueous solution of KPF_6 was added to the solution. After evaporation of the acetone in a rotary evaporator, a brown-pale solid was obtained and recrystallized from DCM/diethyl ether, yielding brown crystals. Yield: 75%. Anal. Calcd for $C_{49}H_{39}F_{18}N_{12}P_3Ru_2$: C, 41.07; H, 2.79; N, 11.73. Found: C, 41.02; H, 2.98; N, 11.57. ^{1}H NMR (400 MHz, acetone-d_6, 298 K, ppm): δ 1.09 (wide, 4H, H_P), 2.02 (wide, 4H, H_O), 7.07 (t, $J_{D-E} = J_{D-C} = 7.74$ Hz, 2H, H_D), 7.49 (d, $J_{E-D} = 7.74$ Hz, 2H, H_E), 7.56 (t, $J_{G-H} = J_{G-F} = 8.08$ Hz, 4H, H_G), 7.91 (t, $J_{C-D} = J_{C-B} = 7.74$ Hz, 2H, H_C), 8.17 (t, $J_{H-G} = J_{H-I} = 8.08$ Hz, 4H, H_H), 8.22 (d, $J_{B-C} = 7.74$ Hz, 2H, H_B), 8.43 (t, $J_{K-J} = 8.33$ Hz, 2H, H_K), 8.48 (s, 1H, H_A), 8.72 (d, $J_{I-H} = 8.08$ Hz, 4H, H_I), 8.84 (d, $J_{J-K} = 8.33$ Hz, 4H, H_J). UV−vis (CH_2Cl_2) [λ_{max}, nm (ε, M^{-1} cm^{-1})]: 272 (58 649), 310 (70 955), 356 (26 048), 441 (12 921), 469 (11 808), 546 (2337). $E_{1/2}$ (CH_2Cl_2, V vs SSCE): 1.056, 1.352. MALDI(+)-MS: (CH_2Cl_2): 1290.03 ([M − PF_6]$^+$).

*in,in-{[Ru^{II}(trpy)]$_2$(μ-bpp)(μ-glut)}(PF$_6$)$_3$·2H$_2$O [**6b(PF$_6$)$_3$·2H$_2$O**].* A total of 50 mg (0.032 mmol) of complex *in,in*-{[Ru(trpy)]$_2$(μ-bpp)(μ-AcO)}$(PF_6)_3$ was dissolved in 80 mL of acetone/water (3:1), followed by the addition of 5 mL of a triflic acid aqueous solution (pH = 1). After the addition of 0.08 mL of 1,3-dicyanopropane (glutaronitrile; glut), the mixture was heated under reflux for 3 h. Upon cooling to room temperature, the unreacted starting material was filtered and 1 mL of a saturated aqueous solution of KPF_6 was added to the solution. After evaporation of the acetone in a rotary evaporator, a brown-pale solid was obtained and recrystallized from DCM/diethyl ether, yielding brown crystals. Yield: 73%. Anal. Calcd for $C_{48}H_{41}F_{18}N_{12}O_2P_3Ru_2$: C, 39.62; H, 2.84; N, 11.55. Found: C, 39.80; H, 2.75; N, 11.45. ^{1}H NMR (400 MHz, acetone-d_6, 298 K, ppm): δ 1.33 (q, 2H, H_P), 2.19 (t, 4H, H_O), 7.07 (t, $J_{D-E} = J_{D-C} = 7.74$ Hz, 2H, H_D), 7.49 (d, $J_{E-D} = 7.74$ Hz, 2H, H_E), 7.56 (t, $J_{G-H} = J_{G-F} = 8.08$ Hz, 4H, H_G), 7.91 (t, $J_{C-D} = J_{C-B} = 7.74$ Hz, 2H, H_C), 8.17 (t, $J_{H-G} = J_{H-I} = 8.08$ Hz, 4H, H_H), 8.22 (d, $J_{B-C} = 7.74$ Hz, 2H, H_B), 8.41 (d, $J_{F-G} = 8.08$ Hz, 2H, H_F), 8.43 (t, $J_{K-J} = 8.33$ Hz, 2H, H_K), 8.48 (s, 1H, H_A), 8.72 (d, $J_{I-H} = 8.08$ Hz, 4H, H_I), 8.84 (d, $J_{J-K} = 8.33$ Hz, 4H, H_J). UV−vis (CH_2Cl_2) [λ_{max}, nm (ε, M^{-1} cm^{-1})]: 273 (50 063), 310 (60 140), 354 (21 624), 440 (10 280), 466 (10 168), 546 (2758). $E_{1/2}$ (CH_2Cl_2, V vs SSCE): 1.060, 1.308. MALDI(+)-MS: (MeOH): 1275.1 ([M − PF_6]$^+$).

*in,in-{[Ru^{II}(trpy)]$_2$(μ-bpp)(μ-succ)}(PF$_6$)$_3$·3H$_2$O [**6c(PF$_6$)$_3$·3H$_2$O**].* A total of 50 mg (0.032 mmol) of complex *in,in*-{[Ru(trpy)]$_2$(μ-bpp)(μ-AcO)}$(PF_6)_3$ was dissolved in 80 mL of acetone/water (3:1), followed by the addition of 5 mL of a triflic acid aqueous solution (pH = 1), and was left to stir at room temperature overnight. A total of 3.3 mg (0.032 mmol) of 1,2-dicyanoethane (succinonitrile, succ) was dissolved in 5 mL of water, and the resulting solution was added dropwise over 1 h. Then the mixture was heated under reflux for 2 h. Upon cooling to room temperature, the unreacted starting material was filtered and 1 mL of a saturated aqueous solution of KPF_6 was added to the solution. After evaporation of the acetone in a rotary evaporator, a pale-brownish solid was obtained and recrystallized from DCM/ether, yielding brown crystals. Yield: 66%. Anal. Calcd for $C_{47}H_{41}F_{18}N_{12}O_3P_3Ru_2$: C, 38.69; H, 2.83; N, 11.52. Found: C, 38.46; H, 2.86; N, 11.39. ^{1}H NMR (400 MHz, acetone-d_6, 298 K, ppm):

dx.doi.org/10.1021/ic202225g | Inorg. Chem. 2012, 51, 1889−1901

δ 2.71 (s, 4H, H_O), 7.07 (t, $J_{D-E} = J_{D-C} = 7.74$ Hz, 2H, H_D), 7.49 (d, $J_{E-D} = 7.74$ Hz, 2H, H_E), 7.56 (t, $J_{G-H} = J_{GF} = 8.08$ Hz, 4H, H_G), 7.91 (t, $J_{C-D} = J_{C-B} = 7.74$ Hz, 2H, H_C), 8.17 (t, $J_{H-G} = J_{H-I} = 8.08$ Hz, 4H, H_H), 8.22 (d, $J_{B-C} = 7.74$ Hz, 2H, H_B), 8.43 (t, $J_{K-J} = 8.33$ Hz, 2H, H_K), 8.48 (s, 1H, H_A), 8.53 (d, $J_{F-G} = 8.08$ Hz, 4H, H_F), 8.72 (d, $J_{I-H} = 8.08$ Hz, 4H, H_I), 8.84 (d, $J_{J-K} = 8.33$ Hz, 4H, H_J). UV−vis (CH_2Cl_2) [λ_{max}, nm (ε, M^{-1} cm^{-1})]: 272 (49 246), 310 (58 844), 356 (22 176), 444 (11 173), 471 (10 214), 546 (2313). $E_{1/2}$ (CH_2Cl_2, V vs SSCE): 1.076, 1.328. MALDI(+)-MS (MeOH): 1261.1 ($[M - PF_6]^+$).

Equipment and Measurements. All electrochemical experiments were performed in a PAR 263A EG&G potentiostat or in a IJ-Cambria IH-660 potentiostat, using a three-electrode cell. Glassy carbon (3 mm diameter) from BAS was used as the working electrode, a platinum wire as the auxiliary electrode, and SSCE as the reference electrode. Cyclic voltammograms were recorded at a 100 mV s^{-1} scan rate under a nitrogen atmosphere. The complexes were dissolved in previously degassed DCM containing the necessary amount of (n-Bu_4N)(PF_6), used as the supporting electrolyte, to yield a 0.1 M ionic strength solution. All $E_{1/2}$ values reported in this work were estimated from cyclic voltammetry (CV) as the average of the oxidative and reductive peak potentials ($E_{p,a} + E_{p,c}$)/2 or from differential pulse voltammetry (DPV; pulse amplitudes of 0.05 V, pulse widths of 0.05 s, sampling width of 0.02 s, and a pulse period of 0.1 s). Unless explicitly mentioned, the concentrations of the complexes were approximately 1 mM. A 400 MHz Bruker avance II spectrometer was used to carry out NMR spectroscopy at room temperature. At low temperatures, a Bruker Avance 500 MHz spectrometer was used. Samples were run in CD_2Cl_2, acetone-d_6, or acetonitrile-d_3. The electrospray ionization and matrix-assisted laser desorption ionization (MALDI) mass spectrometry (MS) experiments were performed on a Waters Micromass LCT Premier equipment and a Bruker Daltonics Autoflex equipped with a nitrogen laser (337 nm), respectively. UV−vis spectroscopy was performed on a Cary 50 Bio (Varian) UV−vis spectrophotometer with 1 cm quartz cells.

UV−vis kinetic studies on the ligand-substituted processes were performed at various concentrations of the dinuclear complex and always using acetonitrile as the solvent. In a typical experiment, a solution of the starting complex at concentrations varying from 5 to 350 μM was prepared at 0 °C and introduced to the quartz cells, which where preheated at the desired temperature; typically, a full spectrum was recorded every 10 min. In all cases, the temperature was maintained at ±0.1 °C with a Huber CC3-905 VPCw cryostat. First- and second-order rate constants were calculated by a global-fitting method or a single-wavelength fitting using *Specfit*.[14] The data were reproduced by two first-order consecutive reactions (A → B → C). In all cases, rate constants were measured at four different temperatures.

Single-Crystal X-ray Structure Determination. *Crystal Preparation.* Crystals for $\mathbf{3a}^{n+}$ were grown by the slow diffusion of diethyl ether into an acetonitrile solution of the complex. Crystals for complexes $\mathbf{3b}^{3+}$, $\mathbf{4}^{3+}$, $\mathbf{6a}^{3+}$, and $\mathbf{6c}^{3+}$ were grown by the slow diffusion of diethyl ether into an acetone solution of the complex. Crystals for complex $\mathbf{3c}^{3+}$ were grown from MeCN at 4 °C. All measured crystals were prepared under inert conditions immersed in perfluoropolyether as the protecting oil for manipulation. Crystals of $\mathbf{3a}^{n+}$, $\mathbf{3b}^{3+}$, $\mathbf{3c}^{3+}$, $\mathbf{4}^{3+}$, and $\mathbf{6a}^{3+}$ were measured at −173.2 °C, and the crystal of $\mathbf{6c}^{3+}$ was measured at room temperature.

Data Collection. Crystal structure determinations for complexes $\mathbf{3a}^{n+}$, $\mathbf{3b}^{3+}$, $\mathbf{3c}^{3+}$, $\mathbf{4}^{3+}$, $\mathbf{6c}^{3+}$, and $\mathbf{6a}^{3+}$ were carried out using a Bruker Nonius diffractometer equipped with an APEX II 4K CCD area detector, a FR591 rotating anode with Mo Kα radiation, Montel mirrors as a monochromator, and a Kappa 4-axis goniometer. Low-temperature measurements were performed using a Kryoflex low-temperature device (T = −173 °C). Full-sphere data collection was used with ω and φ scans. Programs used: data collection, *APEX-2*;[15] data reduction, Bruker *SAINT V/.60A*;[16] absorption correction, *SADABS*[17] or *TWINABS*.[18]

Structure Solution and Refinement. Crystal structure solutions were achieved using direct methods as implemented in *SHELXTL*[19] and visualized using the program *XP*. Missing atoms were subsequently located from difference Fourier synthesis and added to the atom list. Least-squares refinement on F^2 using all measured intensities was carried out using the program *SHELXTL*. All non-H atoms were refined including anisotropic displacement parameters. The crystal data parameters are listed in Tables 1 and 2. Compound $\mathbf{3a}^{n+}$ crystallized as an acetonitrile solvate. Compound $\mathbf{3b}^{3+}$ crystallized as an acetone/water solvate. One of the acetone molecules is disordered in three positions with a ratio of 33:33:33. The water molecule is disordered in two positions (ratio 50:50). The crystal selected for compound $\mathbf{3c}^{3+}$ turned out to be a twin, which was processed with *RLATT/SAINT* (simultaneous data processing) and *TWINABS* for absorption correction. The structure was refined, taking into account overlapping reflections (crystal ratio 58:42). This compound is an acetonitrile/water solvate (one molecule of acetonitrile and a half molecule of water). The acetonitrile molecule is disordered in three positions (ratio 58:27:15). Compound $\mathbf{4}^{3+}$ crystallized as a diethyl ether/acetone solvate with one molecule of diethyl ether and one molecule of acetone in the asymmetric unit. The structure obtained corresponds to a mixture (90:10) of the complex with two pyridine molecules linked to the Ru atoms and the complex with one acetonitrile and one pyridine linked to the Ru atoms. Because of this occupational disorder, one of the terpyridines rests on the complex and one of the PF_6^- anions is disordered in two orientations/positions with a ratio of 90:10. Additionally, the PF_6^- anions are rotationally disordered. Compound $\mathbf{6c}^{3+}$ was measured at room temperature because crystals were showing degradation due to cooling at low temperatures. The asymmetric unit contains one acetone molecule, which is disordered in two orientations (ratio 60:40). Also, one of the PF_6^- anions is disordered in two orientations (ratio 53:47). For compound $\mathbf{6a}^{3+}$, only extremly small crystals were available. After several atempts, a data set using extremly long acquisition times could be collected and could be refined to acceptable R values. The crystal measured corresponded to an acetone solvate with four molecules of solvent in the asymmetric unit. Two of the acetone molecules are disordered in two orientations (ratio 58:42 and 56:44)

Computational Methods. Calculations on the reaction mechanism were carried out with the *Gaussian03* suite of programs,[20] using the ONIOM method[21,22] at the ONIOM(B3LYP:HF)//ONIOM-(B3LYP:UFF) level of theory.[23,24] The SDD basis set and effective core potential were used to describe Ru atoms,[25] while 6-31G(d)[26,27] was used for all remaining atoms. The ONIOM partitioning is shown in the Figure S5.1 in the Supporting Information. H atoms were used to cap the bonds that cross the partition between the high and low levels. Because the substitution reactions occur at different metal centers, there is a discontinuity in the reaction profile because the metal center involved in the substitution reaction must be modeled with DFT. This means that *in*,*in*-{[Ru^{II}(trpy)(py)](μ-bpp)[Ru^{II}(trpy)-(MeCN)]}$^{3+}$ ($\mathbf{4}^{3+}$) can be described by two ONIOM partitions, depending on which reaction is of interest. However, the relative energies of the two processes can be compared without problems.

Minima were confirmed through frequency calculations. Both potential and free energies are reported. Relative potential energies correspond roughly to what experimental enthalpy differences would be at 0 K. There is currently significant discussion about how to better estimate entropy corrections for dissociation reactions in solution,[28] with some authors suggesting that the entropy corrections should be halved.[29] Therefore, the true free energy of dissociation lies between the predicted potential and free-energy values. Because the free-energy correction is very similar for the two substitution reactions in this study, we can assume that the errors are similar for both and that a comparison of the two reactions is still very useful.

Solvent effects for the model system were calculated using the polarizable continuum model model[30] with UAHF radii, through single-point Hartree−Fock calculations on the ONIOM-optimized geometries. Calculations were carried out using the experimental solvent acetonitrile.

An additional set of calculations on the pyridine−pyridine and lutidine−lutidine interactions was carried out using the *ORCA 2.7* package.[31] Apart from the B3LYP functional,[20,23] these calculations were also carried out with dispersion-corrected DFT (DFT-D), as implemented in *ORCA*, which uses a semiempirical correction

dx.doi.org/10.1021/ic202225g | *Inorg. Chem.* 2012, 51, 1889−1901

Table 1. Crystal Data for Compounds $3a^{n+}$, $3b^{3+}$, $3c^{3+}$, 4^{3+}, $6a^{3+}$, and $6c^{3+}$

	$3a^{n+}$	$3b^{3+}$	$3c^{3+}$	4^{3+}	$6a^{3+}$	$6c^{3+}$
empirical formula	$C_{55}H_{42}N_{18}O_3Ru_2$	$C_{62}H_{61}F_{18}N_{12}O_4P_3Ru_2$	$C_{61}H_{56}Cl_3N_{14}O_{12.5}Ru_2$	$C_{56.7}H_{54.8}F_{18}N_{12}O_2P_3Ru_2$	$C_{61}H_{63}F_{18}N_{12}O_4P_3Ru_2$	$C_{50}H_{41}F_{18}N_{12}O_1P_3Ru_2$
solvent detected	1 ACN	3 acetone + 1 water	1 ACN + $^1/_2$ water	1 diethyl ether + 1 acetone	4 acetone	1 acetone
fw	1205.21	1675.28	1493.69	1573.38	1665.28	1463.00
cryst size (mm^3)	0.10 × 0.05 × 0.02	0.20 × 0.20 × 0.05	0.10 × 0.10 × 0.05	0.10 × 0.15 × 0.05	0.15 × 0.10 × 0.05	0.40 × 0.15 × 0.05
cryst color	purple	brown	brown	brown	yellow	green
temp (K)	100	100	100	100	100	298
cryst syst	monoclinic	triclinic	triclinic	monoclinic	triclinic	monoclinic
space group	$P2_1/n$	$P\bar{1}$	$P\bar{1}$	$P2_1/n$	$P\bar{1}$	$P2_1/c$
a (Å)	15.5976(7)	14.5367(6)	13.2188(3)	13.2129(4)	12.1634(6)	8.9364(12)
b (Å)	14.0158(7)	15.9696(6)	15.9950(5)	19.9774(5)	14.6606(8)	39.603(7)
c (Å)	23.0456(11)	17.9748(7)	16.5739(5)	23.3886(6)	20.4082(10)	16.206(3)
α (deg)	90	92.694(2)	73.2580(10)	90	98.513(3)	90
β (deg)	98.178(2)	110.779(2)	74.3300(10)	93.961(2)	105.328(3)	95.571(6)
γ (deg)	90	113.366(2)	69.0450(10)	90	101.768(3)	90
V (Å^3)	4986.8(4)	3494.7(2)	3078.64(15)	6158.9(3)	3356.5(3)	5708.5(16)
Z	4	2	2	4	2	4
ρ (g cm^{-3})	1.605	1.592	1.611	1.697	1.648	1.702
μ (mm^{-1})	0.673	0.604	0.697	0.677	0.628	0.722
θ_{max} (deg)	39.34	36.40	27.34	39.57	25.20	36.42
reflns measd	112 371	76 263	24 281	129 144	66 462	117 626
unique reflns obsd	22 222 [R_{int} = 0.0385]	19 842 [R_{int} = 0.0416]	5446 [R_{int} = 0.0857]	14 161 [R_{int} = 0.0986]	8211 [R_{int} = 0.1077]	13 442 [R_{int} = 0.0843]
abs corrn	*SADABS*	*SADABS*	*TWINABS*	*SADABS*	*SADABS*	*SADABS*
trans min/max	0.95/1.00	0.92/1.00	0.97/1.00	0.94/1.00	0.94/1.00	0.79/1.00
no. of param	706	931	872	1142	959	831
R1/wR2 [$I > 2\sigma(I)$]	0.0593/0.1372	0.0621/0.1737	0.0566/0.1096	0.0555/0.1267	0.0949/0.2618	0.0647/0.1639
R1/wR2 [all data]	0.0824/0.1496	0.1021/0.2077	0.1114/0.1324	0.1085/0.1530	0.1393/0.2618	0.1444/0.2040
GOF (F^2)	1.128	1.024	1.009	1.031	1.092	1.008
peak/hole (e Å^{-3})	2.556/−3.147	1.935/−1.300	0.979/−0.941	1.753/−1.153	1.891/−1.405	1.102/−1.075

Table 2. Selected Metric Parameters (Distances in Angstroms and Angles in Degrees) for the Complexes Described in This Paper Together with Related Complexes for Comparison Purposes

complex	RuNNRu[a]	py-py′(bpp$^-$)[b]	py-py′(L)[c]	dc[d]
$\mathbf{3b}^{3+}$	45.7	22.3	6.5	3.48
$\mathbf{3c}^{3+}$	26.8	15.9	2.3	3.34
$\mathbf{4}^{3+}$	44.7	20.4		3.52
$\mathbf{3a}^{3+}$ [e]	53.2	25.9		3.27
$\mathbf{3d}^{n+}$ [e]	44.3	17.5	0.8	3.52
$\mathbf{3a}^{n+}$	44.5	17.6		3.28
$\mathbf{6a}^{3+}$	40.12	9.20		3.01
$\mathbf{6c}^{3+}$	55.56	28.31		2.68

[a]Dihedral angle that involves the two N atoms belonging to the pyrazolate-bridged group of the bpp$^-$ ligand and two metal centers. [b]Angle between the pyridyl groups of the bpp$^-$ anionic ligand. [c]Angle between the best planes that run through the pyridylic monodentate ligands. [d]Distance between the centroids of the two monodentate pyridyl rings. The C atom of the nitrile group is used in the case of complexes containing MeCN monodentate ligands or NC−$(CH_2)_n$−CN bridging [e]For complexes $\mathbf{3a}^{3+}$ and $\mathbf{3d}^{n+}$, see ref 9.

proposed by Grimme[32] to account for van der Waals forces. The TZVP basis set[33] was used for this additional set of calculations.

RESULTS AND DISCUSSION

Synthesis and Structure. The synthetic strategy, followed for the preparation of the complexes described here, is depicted in Scheme 2. The addition of the octahedral ruthenium complex $[H_xTRu^{III}Cl_3]$ (T = trpy, x = 0; T = bid$^-$, x = 1) to the tetraaza dinucleating Hbpp ligand in the presence of NEt_3 generates the corresponding dinuclear ruthenium complexes $\mathbf{1}^{2+}$ and $\mathbf{1}'$ with C_{2v} and C_s symmetry, respectively. Whereas for $\mathbf{1}^{2+}$ the monodenate Cl ligand acts as a bridging ligand for $\mathbf{1}'$, the Cl simply acts as a nonbridging monodentate ligand to one of the Ru centers while the second center is coordinated by a MeOH. For easy followup of the complex nomenclature in this paper, all complexes containing the anionic bid$^-$ ligand are denoted with a prime, whereas the ones with trpy are not. The subsequent reactions of $\mathbf{1}^{2+}$ or $\mathbf{1}'$ with an acetate anion generate the corresponding $\mathbf{2}^{2+}$ and $\mathbf{2}'$ complexes (both with C_2 symmetry), which contain two bridging ligands, the original bpp$^-$ and the acetato that acts now as a bidentate ligand bridging the two Ru metal centers. These acetato bridge complexes are excellent starting materials because they are easy-to-handle crystalline materials that are obtained with relatively reasonable yields. In addition, the lability of the acetato bridge allows one to easily obtain the family of $\mathbf{3}^{3+}$, $\mathbf{3}^{n+}$, and $\mathbf{6}^{3+}$complexes containing the corresponding monodentate (L) or bridging (μ-L-L) ligands. Complex $\mathbf{4}^{3+}$, which contains mixed monodentate ligands, can be obtained by careful control of the reaction time using the bis(pyridyl) complex $\mathbf{3b}^{3+}$ as the starting material, using acetonitrile as the solvent.

X-ray crystal structures have been obtained for complexes $\mathbf{3a}^{n+}$, $\mathbf{3b}^{3+}$, $\mathbf{3c}^{3+}$, $\mathbf{4}^{3+}$, $\mathbf{6a}^{3+}$, and $\mathbf{6c}^{3+}$. Their most relevant crystallographic parameters are reported in Tables 1 and 2, whereas their molecular plots are shown in Figure 1 or in the Supporting Information. All Ru−N bond distances and angles are within the typical values for octahedral $Ru^{II}N_6$ d^6 types of cations.[34]

dx.doi.org/10.1021/ic202225g | Inorg. Chem. 2012, 51, 1889−1901

Scheme 2. Synthetic Strategy[a]

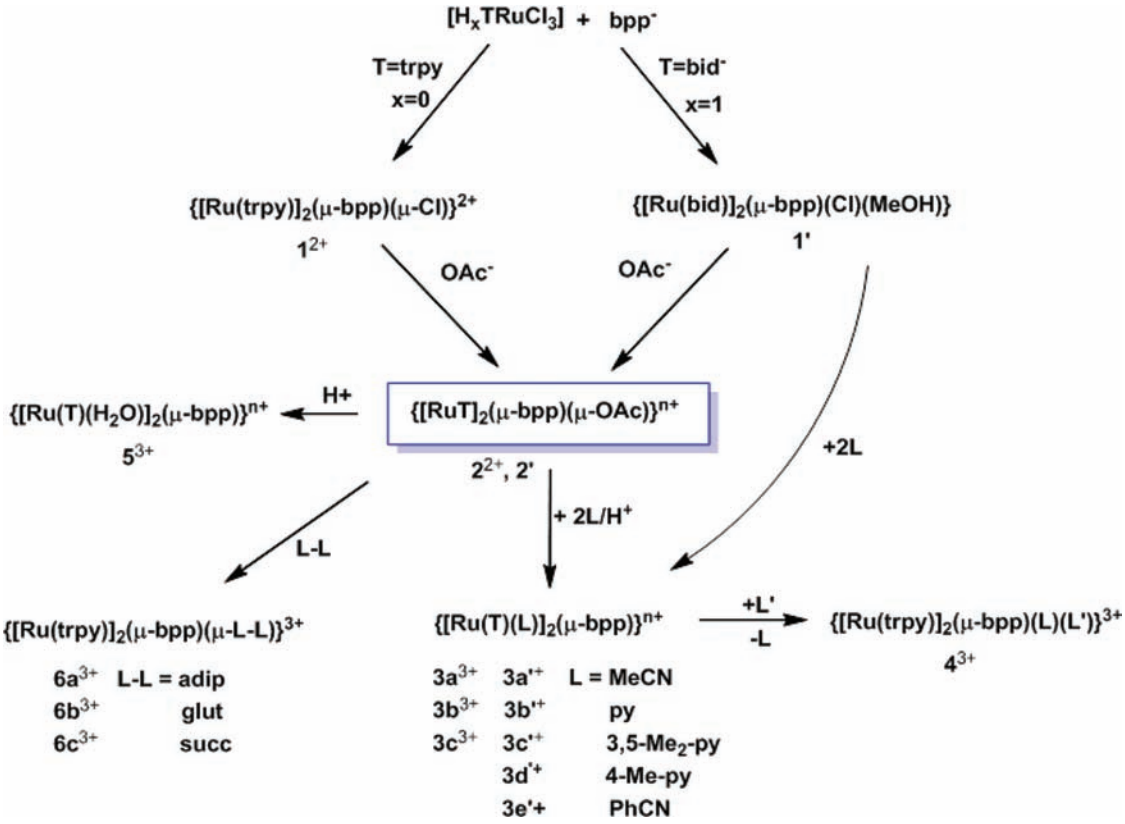

[a]Complexes containing the prime refer to the ones that contain the bid$^-$ ligand, whereas those that do not have the prime contain the trpy ligand.

The Ru centers possess an octahedrally distorted coordination geometry as a consequence of the steric encumbrance provoked by the mutual interaction of the monodentate ligands, which forces them to accommodate above and below an ideal equatorial plane. As a result, all complexes possess C_2-type symmetry, and their optical image counterpart can also be found in each unit cell. At room temperature in solution, the two enantiomers indicated in eq 3 interconvert very fast. In order to quantify the degree of distortion of the octahedral geometry around the Ru centers, two parameters have been measured and are reported in Table 2: (a) the RuNNRu dihedral angle, where N belongs to the N atoms of the pyrazolate group of the bpp$^-$ ligand, and (b) the py-py′ (bpp$^-$) angle, which is the angle between the best planes described by the pyridyl groups of the bpp$^-$ ligand. As can be observed in Table 2, the RuNNRu angle ranges from 40° to 56° for all complexes except for **3c**$^{3+}$ containing the lutidine ligand, for which the angle is only 26.8°. For the py-py′ (bpp$^-$) case, the angles range from 17° to 24° for the complexes containing monodentate ligands. The lutidinde complex **3c**$^{3+}$ has the lowest value. These two parameters clearly indicate that in the lutidine complex the degree of distortion is lower than that in any of the other complexes containing monodentate ligands. It is also interesting to observe that the adiponitrile **6a**$^{3+}$ complex has the lowest distortion among the dinitrile complexes. On the other hand, the shortening of the alquilic chain of the dinitrile ligand produces a substantial increase of distortion of the first coordination sphere of the Ru metal centers due to an increase of the rigidity of the dinitrile ligand, as can be seen in the X-ray structures of complexes **6a**$^{3+}$ and **6c**$^{3+}$.

Another interesting structural feature of the present complexes is the nearly parallel disposition of the aromatic rings of the monodentate ligands containing pyridyl-type monodentate ligands, as can also be seen in Table 2, which indicates a certain degree of $\pi-\pi$ interaction. Whereas for complex **3b**$^{3+}$ the aromatic rings are slightly rotated with regard to one another, for the **3c**$^{3+}$ complex, the aromatic rings are situated in an eclipsed manner, as can be observed in Figure 1, middle left. All of these particularities associated with the lutidine complex point out the existence of a certain degree of attractive interaction between the aromatic rings, which will be further discussed later on.

Spectroscopic, Redox Properties, and Dynamic Behavior. 1D and 2D NMR spectroscopy allowed one to fully characterize the structures of all ruthenium(II) complexes in solution, which, as expected, coincided with their solid-state structures. The ^{1}H NMR aromatic regions for **3a**$^{3+}$, **3b**$^{3+}$, and **4**$^{3+}$ are plotted in Figure 2, whereas the rest of the 1D and 2D NMR spectra for this and all of the other complexes described in this work are presented as Supporting Information. An interesting feature of these complexes that is reflected in NMR spectroscopy at low temperatures is the relative rotation of the meridional trpy and bid$^-$ ligands needed to accommodate the monodentate or dicyano bridging ligands. This produces an upfield shift of the external pyridyl of trpy, the H_F proton, whereas the opposite external H_F′ proton suffers a downfield shift[10] (see Supporting Information). Finally, it is also worth mentioning here that the Me group of the monodentate MeCN ligand in the mixed-ligand complex **4**$^{3+}$ has a 0.17 ppm shift with regard to the bis-MeCN, **3a**$^{3+}$, due to the interaction of the Me group with the aromatic ring current of the pyridine ligand.

dx.doi.org/10.1021/ic202225g | Inorg. Chem. 2012, 51, 1889−1901

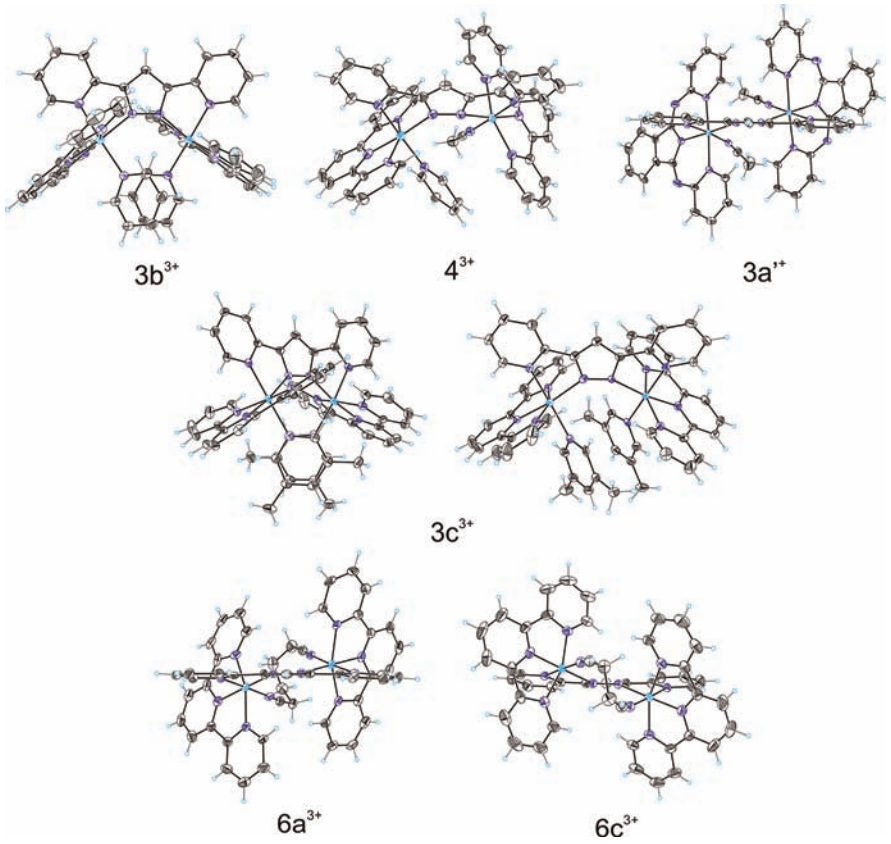

Figure 1. ORTEP diagrams (50% probability) for the molecular structure of the cationic parts of complexes $\mathbf{3b}^{3+}$, $\mathbf{4}^{3+}$, $\mathbf{3a}'^{4+}$, $\mathbf{3c}^{3+}$, $\mathbf{6a}^{3+}$, and $\mathbf{6c}^{3+}$ obtained from X-ray diffraction analysis. Color code: Ru, cyan; N, blue; C, gray; H, light blue.

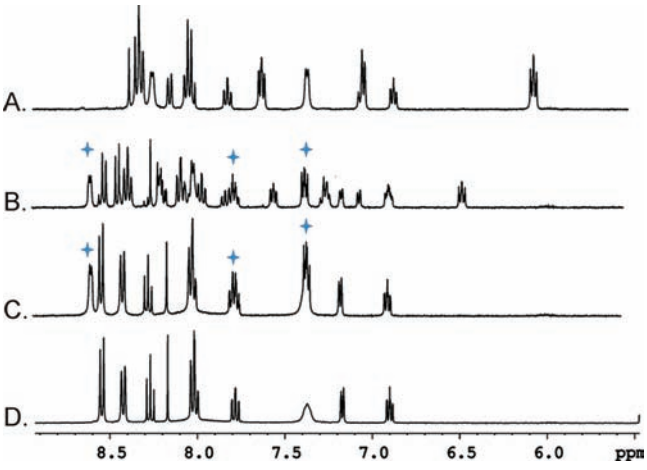

Figure 2. ^{1}H NMR spectra. (A) $\mathbf{3b}^{3+}$ (6×10^{-3} M in MeCN-d^3) taken after 10 min at room temperature. (B) $\mathbf{4}^{3+}$ formed by dissolving $\mathbf{3b}^{3+}$ in MeCN-d^3 after 7 h at 70 °C. The stars indicate free pyridine resonances. (C) $\mathbf{3a}^{3+}$ formed by dissolving $\mathbf{3b}^{3+}$ in MeCN-d^3 after 15 h at 70 °C. (D) $\mathbf{3a}^{3+}$ in MeCN-d^3 obtained from an authentic sample. The assignment of all resonances can be found in the Experimental Section.

As mentioned earlier, all of the complexes described in this work present a dynamic behavior at room temperature because of interconversion of their corresponding enantiomers, as indicated in eq 3 and reported earlier.[10] However, it is interesting to see the effect of the bridging dinitrile ligands of the family of complexes $\mathbf{6}^{3+}$ on the kinetics of this interconversion that can be investigated via variable-temperature NMR (see Table S1a.1 in the Supporting Information). Complexes with two and three methylenic units, $\mathbf{6b}^{3+}$ and $\mathbf{6c}^{3+}$, interconvert very fast with activation energies lower than 17.5 kJ mol^{-1}. In sharp contrast, when the methylenic chain increases to four units, complex $\mathbf{6a}^{3+}$, the activation barrier rises to 51.0 kJ mol^{-1}, manifesting the difficulty of reorganizing the alquilic chain between the two enantiomeric forms.

The family of $\mathbf{3}^{3+}$ and $\mathbf{3}'^{4+}$ complexes described in the present work contain strongly bonded polydentate ligands that coordinate the Ru^{II} centers and benefit from the chelating effect for extra stability. In sharp contrast, their respective monodentate ligands exchange with coordinating solvents if they are treated at sufficiently high temperatures. As an example, the following equations show the substitution reactions that operate when $\mathbf{3b}^{3+}$ is heated in MeCN (the trpy and bpp^- ligands are not displayed).

$$\underset{\mathbf{3b}^{3+}}{\textit{in,in}\text{-}[Ru_2(py)_2]^{3+}} + MeCN \rightarrow \underset{\mathbf{4}^{3+}}{\textit{in,in}\text{-}[Ru_2(py)(MeCN)]^{3+}} + py \quad (4)$$

$$\underset{\mathbf{4}^{3+}}{\textit{in,in}\text{-}[Ru_2[(py)(MeCN)]^{3+}} + MeCN \rightarrow \underset{\mathbf{3a}^{3+}}{\textit{in,in}\text{-}[Ru_2(MeCN)_2]^{3+}} + py \quad (5)$$

The substitution process can be nicely followed by NMR spectroscopy, as shown in Figure 2, and it is interesting to realize here that the substitution process proceeds very cleanly from $\mathbf{3b}^{3+}$ to $\mathbf{4}^{3+}$ to $\mathbf{3a}^{3+}$ without the presence of any other

dx.doi.org/10.1021/ic202225g | Inorg. Chem. 2012, 51, 1889–1901

Scheme 3. Proposed Reaction Mechanism[a]

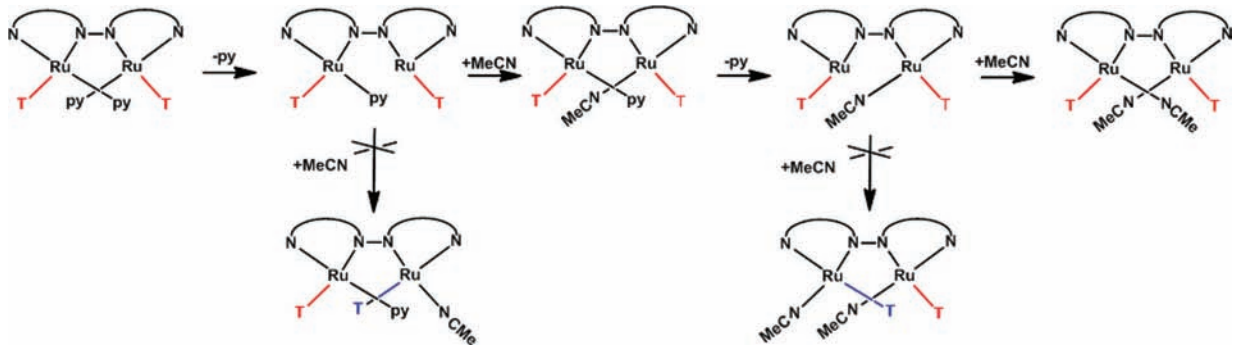

[a]The arcs connecting the four N atoms represent the bpp$^-$ ligand whereas the trpy or bid$^-$ ligands are represented by T. The axial coordination of T ligands is not shown for clarity purposes. The non-occurring potential *in,in* → *in,out* isomerization process is displayed in blue. See text for details.

product at the end of the reaction except for free pyridine. In other words, the *in,in* configuration is maintained in the two substitution reactions, and no isomerization to the potential *in,out* or *out,out* isomers occurs (see Scheme 3).

UV−vis spectroscopy has been recorded both in a non-coordinating solvent such as DCM and in MeCN as a coordinating solvent at room temperature. Figure 3 shows the

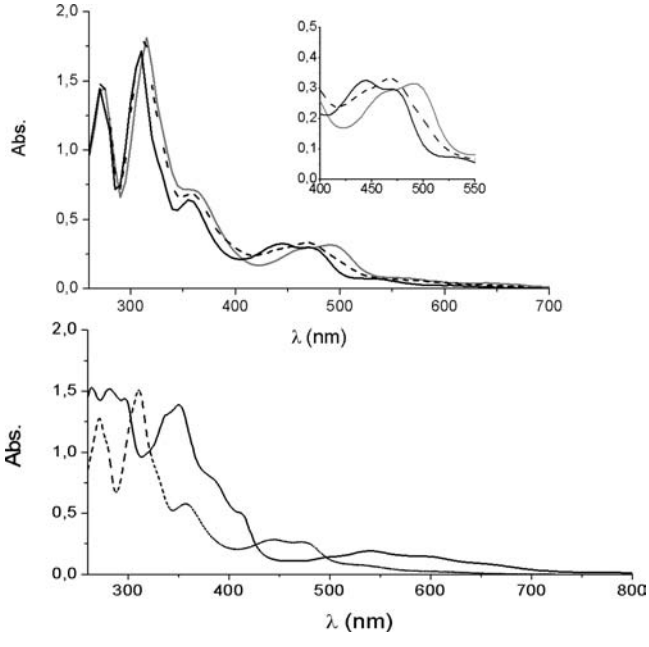

Figure 3. UV−vis spectra in CH_2Cl_2 for 36 μM solutions of complexes: Top, **3a**$^{3+}$ (black solid line), **4**$^{3+}$ (dotted line), and **3b**$^{3+}$ (gray line). The inset shows an enlargement of the 400−550 nm region. Bottom, **3a**$^{3+}$ (dotted line) and **3a**$'^{+}$ (solid line).

spectra for complexes **3a**$^{3+}$, **3b**$^{3+}$, **4**$^{3+}$, and **3a**$'^{+}$, and for the rest of the complexes, their spectra are presented in the Supporting Information. Table 3 contains the most prominent UV−vis spectroscopic features together with their redox potentials. As expected for $Ru^{II}N_6$-type complexes with polypyridylic ligands,[35] they present $\pi-\pi^*$-ligand-based allowed transitions below 300 nm and metal-to-ligand charge-transfer (MLCT) and dd bands above 300 nm. The two MLCT bands that appear in the range of 400−550 nm are particularly interesting because they shift to the blue when the pyridine complex **3b**$^{3+}$ is compared with the MeCN complex **3a**$^{3+}$. The latter is known to produce a stronger back-bonding interaction with Ru, which, in turn, destabilizes dπ(Ru) orbitals, and as a consequence, the two MLCT bands shift to lower energy. This shift is graphically shown in Figure 3, top. For the case of the bid$^-$ complexes, the anionic character of the ligand produces a destabilization of the dπ(Ru) orbitals, which, as a consequence, produces a red shift of the MLCT bands, as shown for complexes **3a**$^{3+}$ and **3a**$'^{+}$ in Figure 3, bottom. Finally, for complexes containing the bid$^-$ ligand, a larger number of $\pi-\pi^*$ bands are observed (see also the Supporting Information for UV−vis spectra of the free ligands).

The energy shifts of the MLCT bands observed in the UV−vis are in agreement with the redox properties displayed by these complexes, which have been studied by means of CV and DPV in CH_2Cl_2. Their cyclic and differential pulse voltammograms are presented in the Supporting Information, whereas their formal redox potentials are shown in the Experimental Section and in Table 3. All of the complexes studied in the present work display two redox processes that are due to two consecutive 1e$^-$ removals. Equations 6 and 7 exemplify the case for **3b**$^{3+}$ (trpy and bpp$^-$ ligands not shown).

$$\underset{\mathbf{3b}^{4+}}{\textit{in,in}\text{-}[Ru^{III}Ru^{II}(py)_2]^{4+}} + 1e^- \rightarrow \underset{\mathbf{3b}^{3+}}{\textit{in,in}\text{-}[Ru^{II}{}_2(py)_2]^{3+}}\ E_{1/2} = 1.34\ (\text{V vs SSCE}) \quad (6)$$

$$\underset{\mathbf{3b}^{5+}}{\textit{in,in}\text{-}[Ru^{III}{}_2(py)_2]^{5+}} + 1e^- \rightarrow \underset{\mathbf{3b}^{4+}}{\textit{in,in}\text{-}[Ru^{III}Ru^{II}(py)_2]^{4+}}\ E_{1/2} = 1.34\ (\text{V vs SSCE}) \quad (7)$$

A first glance at Table 3 shows that, in general, complexes containing the MeCN ligand have slightly higher redox potentials compared to the ones containing the pyridyl ligand, as a consequence of the stronger π-acceptor character of the former with regard to the latter. On the other hand, the replacement of trpy by the bid$^-$ ligand produces a decrease of the redox potentials by about 330 to 450 mV because of anionic character of the latter. It is also worth mentioning that the difference between III,III/III,II and III,II/II,II oscillates between 210 and 320 mV and thus indicates a significant variation of the degree of electronic coupling between the Ru metal centers.

dx.doi.org/10.1021/ic202225g | *Inorg. Chem.* 2012, 51, 1889−1901

Table 3. UV−Vis Spectroscopic Features and Redox Properties for Complexes 3^{3+}, 3^{n+}, 4^{3+}, and 6^{3+} Recorded in DCM

complex	UV−vis: λ_{max}, nm (ε, M^{-1} cm^{-1})	$E_{1/2}$[a] (V) III,II → II,II	$E_{1/2}$[a] (V) III,III → III,II	$\Delta E_{1/2}$ (mV)
$\mathbf{3b}^{3+}$	464 (12 867), 498 (11 730)	1.05	1.34	290
$\mathbf{4}^{3+}$	271 (55 806), 312 (66 667), 356 (24 028), 440 (9127), 469 (11 727), 495 (8533), 574 (1856)	1.09	1.34	250
$\mathbf{3a}^{3+}$	272 (59 626), 311 (70 425), 359 (26 803), 444 (13 238), 476 (11 874), 541 (3154).	1.08	1.40	320
$\mathbf{3c}^{3+}$	275 (54 000), 317 (62 450), 361 (25 704), 470 (9412), 502 (10 059), 566 (2439), 660 (1009).	1.04	1.29	250
$\mathbf{3b}^{n+}$	524 (2129), 574 (2760), 646 (2157), 717 (1850)	0.72	0.98	260
$\mathbf{3a}^{n+}$	265 (42 331), 284 (41 836), 229 (39 517), 341 (36 757), 352 (38 303), 382 (22 132), 414 (13 346), 503 (4005), 540 (5290), 598 (4062)	0.74	0.95	210
$\mathbf{3d}^{n+}$	530 (2939), 576 (3794), 650 (2984), 723 (1586)	0.70	0.95	250
$\mathbf{6a}^{3+}$	272 (58 649), 310 (70 955), 356 (26 048), 441 (12 921), 469 (11 808), 546 (2337).	1.06	1.35	290
$\mathbf{6b}^{3+}$	273 (50 063), 310 (60 140), 354 (21 624), 440 (10 280), 466 (10 168), 546 (2758).	1.06	1.31	250
$\mathbf{6c}^{3+}$	272 (49 246), 310 (58 844), 356 (22 176), 444 (11 173), 471 (10 214), 546 (2313).	1.07	1.33	260

[a] $E_{1/2}$ obtained from DPV (pulse amplitudes of 0.05 V, pulse widths of 0.05 s, sampling width of 0.02 s, and a pulse period of 0.1 s) reported vs SSCE.

Substitution Reaction Kinetics. Thermal substitution kinetics of $\mathbf{3b}^{3+}$, $\mathbf{3b}^{n+}$, and $\mathbf{3c}^{3+}$ to their corresponding MeCN derivatives $\mathbf{3a}^{3+}$ and $\mathbf{3a}^{n+}$ have been thoroughly studied at different temperatures and complex concentrations in neat MeCN by UV−vis repetitive scans, using *Specfit* to fit the data and extract kinetic and thermodynamic parameters. For specific cases, the kinetics were also followed by ^{1}H NMR spectroscopy, and both methods gave fully consistent results. Furthermore, as mentioned earlier, NMR spectroscopy clearly showed that no reactions other than the nitrile substitution processes take place under the conditions studied here.

In all cases, the data could be fitted with a simple model involving two consecutive reactions with first-order rate constants, as indicated in eqs 4 and 5 for the $\mathbf{3b}^{3+}$ case. Further, we have also studied the substitution process in 1,2-dichloroethane, a noncoordinating solvent. At 66.3 ± 0.1 °C, the rate constants for the substitution reaction are independent of [MeCN] in a range of [Ru]:[MeCN] = 1:2 to 1:1100 (see the Supporting Information). This indicates that dissociation of the pyridyl ligand to form a five-coordinate intermediate is the rate-determining step and that the five-coordinate intermediate quickly reacts with MeCN to finally generate complex $\mathbf{4}^{3+}$. Thus, the first substitution reaction follows the rate law "$v = k_1[\mathbf{3b}^{3+}]$", whereas the second one follows "$v = k_2[\mathbf{4}^{3+}]$".

Figure 4 shows the spectral changes that occur every 10 min for a 6.1 × 10^{-5} M solution of complex $\mathbf{3b}^{3+}$ in MeCN at 66.3 °C, and a plot of absorbance versus time at λ_{max} = 438 nm is shown in the inset. Mathematical treatment of the data gives k_1 = 7.5 × 10^{-4} s^{-1} and k_2 = 8 × 10^{-5} s^{-1} and shows that the first process is about 1 order of magnitude faster than the second one.

Evaluation of the rate constants at different temperatures allowed us to calculate enthalpies and entropies of activation for the two consecutive processes from their corresponding Eyring plots. Rate constants at 20 and 40 °C and the corresponding activation parameters for the three complexes are reported in Table 4, whereas the Eyring plots are presented as Supporting Information.

A first glance at Table 4 shows that, in general, the first substitution reaction, k_1, is faster than the second one, k_2, for the three systems studied here. In particular, at 40 °C for $\mathbf{3b}^{n+}$, k_1 is more than 2 orders of magnitude higher than k_2, whereas for $\mathbf{3b}^{3+}$, they differ a little more than 1 order of magnitude. Finally, for $\mathbf{3c}^{3+}$, k_1 is about 2 times larger than k_2. A second trend that can be deduced from Table 4 is that the complex that contains the anionic bid^- ligand, $\mathbf{3b}^{n+}$, has much larger rate constants than the ones containing the trpy ligand. In particular, k_1 at 293 K for $\mathbf{3b}^{n+}$ is

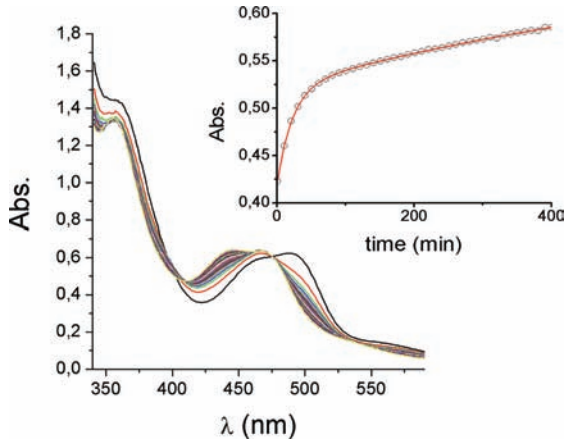

Figure 4. Kinetic profile for the reaction of $\mathbf{3b}^{3+}$ (61 μM) in MeCN at 66.3 °C monitored by UV−vis spectroscopy. Inset: plot of the 438 nm absorbance vs time (black circles) together with the fit (solid red line). See the text for details.

more than 2 orders of magnitude higher than that for $\mathbf{3b}^{3+}$; this phenomenon is clearly linked to the stronger σ-donation capacity of bid^-, as shown also by UV−vis spectroscopy and electrochemistry, vide supra.[36] The substituion kinetics enhancement, associated with strong σ-donating ligands, is a phenomenon that is well documented in the literature for related ruthenium(II) complexes.[36,37]

DFT Calculations on the Substitution Mechanism. Geometric optimization of complexes $\mathbf{3b}^{3+}$, $\mathbf{4}^{3+}$, and $\mathbf{3a}^{3+}$ was carried out following the ONIOM methodology described in the Experimental Section. Calculated structures are shown in the Supporting Information and selected structural parameters displayed in Table S5.1 in the Supporting Information. A comparison with experimental values obtained by X-ray diffraction analysis shows excellent agreement. The substitution reactions indicated in eqs 8 and 9 were also explored by ONIOM calculations. For this purpose, the reaction was divided into two steps as follows:

First Substitution

$$\underset{\mathbf{3b}^{3+}}{\textit{in, in}\text{-}[Ru_2(py)_2]^{3+}} \rightarrow \textit{in}\text{-}[Ru_2(py)]^{3+} + py \quad (8a)$$

$$\textit{in}\text{-}[Ru_2(py)]^{3+} + MeCN \rightarrow \underset{\mathbf{4}^{3+}}{\textit{in, in}\text{-}[Ru_2(py)(MeCN)]^{3+}} \quad (8b)$$

dx.doi.org/10.1021/ic202225g | Inorg. Chem. 2012, 51, 1889−1901

Table 4. Rate Constants Calculated at 40 and at 20 °C, Together with Their Corresponding Activation Parameters, for the Two Substitution Reactions

complex	k	$k_{313\ K}$ (s^{-1})	$k_{293\ K}$ (s^{-1})	$\Delta H^{\ddagger}$ (kJ mol^{-1})	$\Delta S^{\ddagger}$ (J mol^{-1} K^{-1})	$\Delta G_{298\ K}^{\ddagger}$ (kJ mol^{-1})
$\mathbf{3b}^{n+}$	k_1	$(1.98 \pm 0.03)\times 10^{-3}$	$(1.6 \pm 0.05) \times 10^{-4}$	93.9 ± 3.9	4 ± 13	95.1
	k_2	$(1.5 \pm 0.3)\times 10^{-5}$	$(6 \pm 0.5) \times 10^{-7}$	133.4 ± 8.3	82 ± 28	157.8
$\mathbf{3b}^{3+}$	k_1	$(2.9 \pm 0.3)\times 10^{-5}$	3×10^{-7} [a]	110.5 ± 11.7	14 ± 36	114.7
	k_2	$(1.7 \pm 0.7)\times 10^{-6}$	7×10^{-9} [a]	129.4 ± 22.1	50 ± 75	144.3
$\mathbf{3c}^{3+}$	k_1	$(3.0 \pm 0.3)\times 10^{-6}$	7×10^{-8} [a]	108.4 ± 6.4	5 ± 20	109.9
	k_2	$(1.5 \pm 0.5)\times 10^{-6}$	3×10^{-8} [a]	106.4 ± 7.3	19 ± 23	112.1

[a] Calculated values from the Eyring equation.

Second Substitution

$$in,in\text{-}[Ru_2(py)(MeCN)]^{3+} \rightarrow in\text{-}[Ru_2(MeCN)]^{3+} + py \quad (9a)$$
($\mathbf{4}^{3+}$)

$$in\text{-}[Ru_2(MeCN)]^{3+} + MeCN \rightarrow in,in\text{-}[Ru_2(MeCN)_2]^{3+} \quad (9b)$$
($\mathbf{3a}^{3+}$)

This dissociative mechanism, where the pyridine dissociates fully before the acetonitrile comes in, was found to provide good agreement with experiment, while we could not locate the transition states corresponding to the alternative associative mechanism, which would require seven-coordination.

Upon dissociation of pyridine, the structures of the intermediates *in*-$[Ru_2(py)]^{3+}$ and *in*-$[Ru_2(MeCN)]^{3+}$ are found to relax to geometries with approximately planar backbone ligands and with the terpyridine ligands in the *out* position. This geometry favors the formation of *in,in* complexes. The coordination at the metal center is closer to octahedral, with one vacant coordination site at the second metal center. Some rearrangement is necessary in the dissociation and coordination of ligands, but this appears to be compensated for by the coordination energy. Dissociation of pyridine was found to occur with a smooth increase in the energy with no transition state.

As shown in Figure 5, substitution reactions 8 and 9 are calculated to be exothermic by 24 and 18 kJ mol^{-1}, respectively.

The potential formation of the *in,out* isomer, as indicated in eq 10, is calculated to be less favorable than the formation of *in,in*-$[Ru_2(py)(MeCN)]^{3+}$ by 25 kJ mol^{-1}, which along with the geometry of the dissociated complex explains why it has not been observed experimentally.

$$in\text{-}[Ru_2(py)]^{3+} + MeCN \rightarrow in,out\text{-}[Ru_2(py)(MeCN)]^{3+} \quad (10)$$
(in,out-$\mathbf{4}^{3+}$)

The calculated activation barriers depend quite heavily on the free-energy corrections, which are very large for the dissociation step, decreasing the dissociation energy from +59 to −6 kJ mol^{-1}. However, entropy corrections are usually overestimated in solution, and the true value is likely to be somewhere between the two. This is discussed in the theoretical section and explains why the potential energies overestimate the experimentally calculated values. Despite the challenges, the differences between the reactions still give valuable insight into the reaction, especially because the free-energy corrections are similar for the two cases.

The experimental $\Delta H^{\ddagger}$ in Table 4 range between 94 and 133 kJ mol^{-1}, in agreement with the breaking of a Ru−N bond, as has been previously reported in the literature for related complexes.[10,38] All of the experimental and kinetic data obtained are in agreement with the mechanism proposed in Scheme 3. Upon heating of the complex, a Ru−N bond from the pyridine monodentate ligand is broken, forming a five-coordinate intermediate. The intermediate quickly reacts with a solvent molecule to generate a mixed monodentate complex ($\mathbf{4}^{3+}$ for the case of $\mathbf{3b}^{3+}$). At this point, two isomers could be obtained: *in,in*-$\mathbf{4}^{3+}$ or *in,out*-$\mathbf{4}^{3+}$. However, only the former is generated because this product is significantly more thermodynamically stable, as has been put forward by DFT calculations. The stronger Ru^{II}−N bond formed by the MeCN ligand (given its higher π-back-bonding character) with regard to the pyridine ligand, together with the through-space effects, is the thermodynamic driving force for the two consecutive substitution reactions. Five-coordinate intermediate complexes are not unusual for ruthenium(II) complexes, and experimental evidence has been found on a number of occasions.[39]

The differences in the overall exothermicity of the substitution reactions can be explained through a reduction in steric crowding upon replacement of pyridine by acetonitrile. This is especially evident when looking at the calculated energy of dissociation. Dissociation of the pyridine ligand in reaction 8a is calculated to be approximately 40 kJ mol^{-1} less endothermic than that in reaction 9a (the corresponding experimental value is 19 kJ mol^{-1}). Because each substitution reaction is chemically identical for the metal center at which the reaction occurs, the difference must be primarily due to the changes in steric crowding between the metal centers. This is clearly more important for the first substitution because even from direct inspection it is possible to see that the intermediate *in,in*-$[Ru_2(py)(MeCN)]^{3+}$ is less sterically crowded than the reactant, *in,in*-$[Ru_2(py)_2]^{3+}$.

The reduction of steric strain through the reaction is reflected in the changes in the bond lengths and angles. There is a consistent decrease of the Ru−N bond lengths from *in,in*-$[Ru_2(py)_2]^{3+}$ to *in,in*-$[Ru_2(MeCN)(py)]^{3+}$ to *in,in*-$[Ru_2(MeCN)_2]^{3+}$. The Ru−Ru and L−L distances also decrease. The Ru−N and Ru−Ru distances are smaller for the five-coordinate intermediate complexes with only one ligand L, *in*-$[Ru_2(py)]^{3+}$, and *in*-$[Ru_2(MeCN)]^{3+}$. All of these results are consistent with a decrease of the unfavorable steric interactions when pyridine is removed. It also suggests that the interaction between the pyridine groups in the *in,in*-$[Ru_2(py)_2]^{3+}$ complex is repulsive, and thus it is destabilized with regard to *in,in*-$[Ru_2(MeCN)_2]^{3+}$.

Finally, the $\Delta\Delta H^{\ddagger}$ values for $\mathbf{3b}^{n+}$ and $\mathbf{3b}^{3+}$, the difference between the first and second processes, are 39.5 and 18.9 kJ mol^{-1}, respectively, whereas for **3c** (L = 3,5-lutidine), it is only 2.0 kJ mol^{-1}. This is a key observation because, as mentioned earlier, the net processes that occur in the two consecutive reactions are exactly the same, that is the breaking of a Ru−N(pyridine) bond and the formation of a Ru−N(acetonitrile) bond. Therefore, the energetic differences must be due to

dx.doi.org/10.1021/ic202225g | Inorg. Chem. 2012, 51, 1889−1901

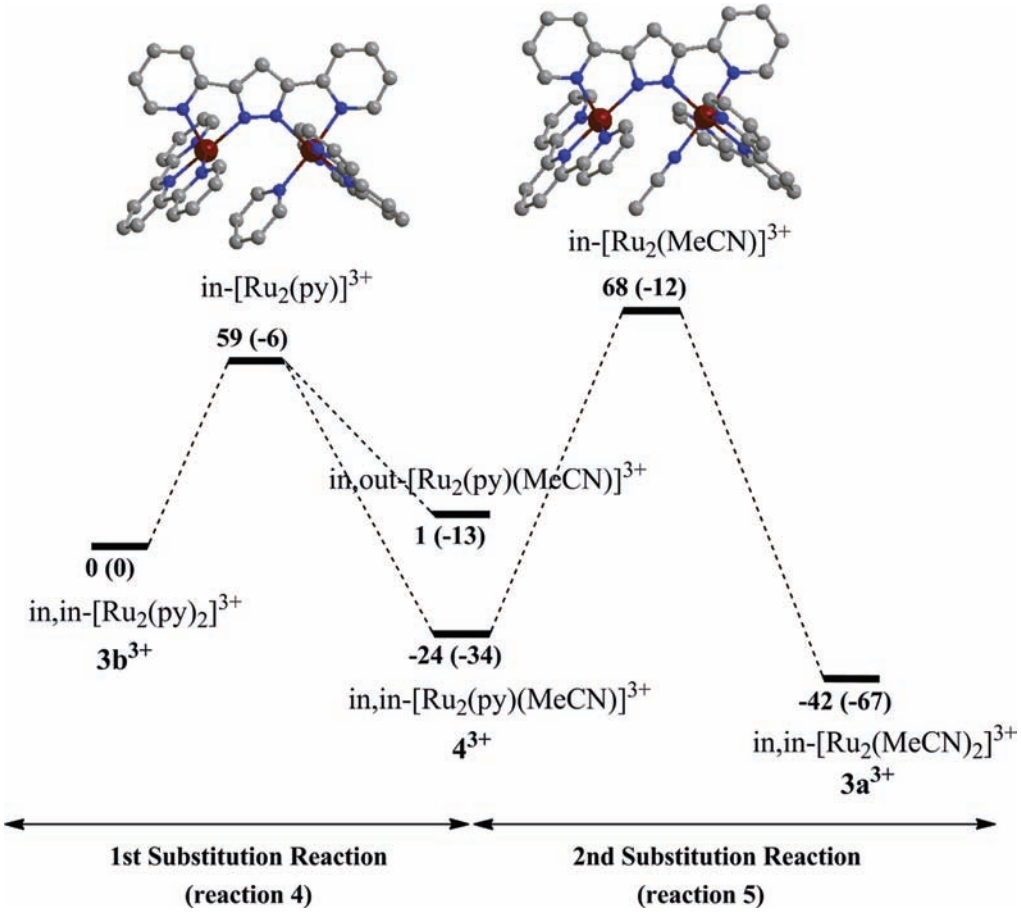

Figure 5. DFT/MM-computed potential energy profile (free energy) in kilojoules per mole for the first and second substitution reactions.

boundary effects. The through-space interaction between the ligands involved was confirmed through an additional set of single-point calculations on the ligands frozen at the geometry that they have in the optimized ruthenium dimers, as shown in Figure 5. The interaction is repulsive at the B3LYP level (23 kJ mol^{-1} for pyridine and 28 kJ mol^{-1} for lutidine) but attractive when dispersion corrections are included at the B3LYP-D level (−7 kJ mol^{-1} for pyridine and −18 kJ mol^{-1} for lutidine). The importance of dispersion corrections is not surprising and adds to the growing number of examples showing their importance.[28] The result is, however, relevant to the topic under discussion because it shows an attraction that is 11 kJ mol^{-1} larger for lutidine than for pyridine. This different behavior justifies the much smaller differences in activation energies for the first and second substitution reactions in the lutidine complex $\mathbf{3c}^{3+}$ with regard to the pyridine complex $\mathbf{3b}^{3+}$. This stronger attractive interaction between the monodentate ligands in the lutidine case, $\mathbf{3c}^{3+}$, is very likely associated with the special spatial arrangement of the monodentate ligands provoked by the bridging bpp^- ligand in combination with the auxiliary trpy ligands. As mentioned earlier in the structural section, for the case of the pyridine and pyridine-substituted ligands, the aromatic rings are situated in a nearly parallel manner. As shown schematically in Figure 6 for complex $\mathbf{3c}^{3+}$, the two lutidines are in a nearly eclipsed conformation and thus have the effect of reducing the eventual steric repulsion between the methyl substituents by favoring attractive interactions, which are likely of C−H π or $\pi-\pi$ nature.

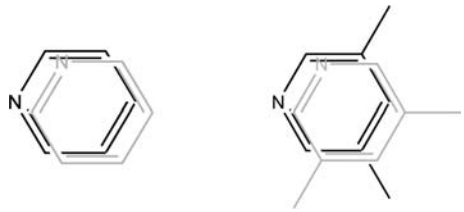

Figure 6. Parallel arrangement of two pyridine rings, left, and two lutidine rings, right, in the structures of $\mathbf{3b}^{3+}$ and $\mathbf{3c}^{3+}$. The rings are rotated 60° with regard to one another.

CONCLUSIONS

We have prepared and characterized a family of complexes containing bridging dinitrile ligands of the general formula *in*,*in*-{[Ru(trpy)]$_2$(μ-bpp)(μ-L-L)}$^{3+}$ [L-L = adiponitrile (adip), glutaronitrile (glut), or succinonitrile (succ)] and have shown how the methylenic chain linking the nitriles is responsible for the activation barriers of their enantiomeric interconversion. Additionally, we have prepared and thoroughly characterized a related family of dinuclear complexes of the general formula *in*,*in*-{[(Ru^{II}(T)(L)]$_2$(μ-bpp)}$^{n+}$ bridged by the bpp^- ligand and containing two additional meridional ligands, the neutral trpy and the anionic bid^-. The final octahedral coordination is occupied by monodentate ligands such as pyridine, substituted pyridines, and MeCN. We have investigated the substitution kinetics of the monodentate ligands, which, in turn, have allowed us to understand the through-space interactions that exist between the monodenate ligands. In the case of

dx.doi.org/10.1021/ic202225g | Inorg. Chem. 2012, 51, 1889−1901

lutidine, the unique and precise disposition of the monodentate ligands shows the existence of an attractive interaction between the ligands. The present work constitutes an example of how dinuclear complexes with the right ligand design can permit precise control of through-space interactions, which can influence both substitution reaction and isomeric interconversions.

■ ASSOCIATED CONTENT

Supporting Information

X-ray crystallographic data in CIF format, detailed experimental procedures together with additional spectroscopic, electrochemical, and kinetic data and *xyz* coordinates for DFT-calculated structures. This material is available free of charge via the Internet at http://pubs.acs.org.

■ AUTHOR INFORMATION

Corresponding Author

*E-mail: fmaseras@iciq.es (F.M.), allobet@iciq.es (A.L.). Fax: 34 977 902 228. Tel: 34977 902 200.

■ ACKNOWLEDGMENTS

Support from MICINN (Grants CTQ2010-21497 and CTQ2008-06866-CO2-02) and from the Consolider Ingenio 2010 (Grant CSD2006-0003) is gratefully acknowledged. N.P. and S.R. are grateful for a MICINN doctoral grant. We thank Dr. Fernando Bozoglian from ICIQ for helpful discussions on kinetics.

■ REFERENCES

(1) (a) Balzani, V.; Bergamini, G.; Ceroni, P. *Coord. Chem. Rev.* **2008**, *252*, 2456−2469. (b) Hang, M.; Huynh, V.; Meyer, T. J. *Chem. Rev.* **2007**, *107*, 5004−5064. (c) Kane-Maguire, N. A. P.; Wheeler, J. F. *Coord. Chem. Rev.* **2001**, *211*, 145−162. (d) Sala, X.; Romero, I.; Rodriguez, M.; Escriche, L.; Llobet, A. *Angew. Chem., Int. Ed.* **2009**, *48*, 2842−2852. (e) Romero, I.; Rodríguez, M.; Sens, C.; Mola, J.; Rao Kollipara, M.; Francàs, L.; Mas-Marza, E.; Escriche, L.; Llobet, A. *Inorg. Chem.* **2008**, *47*, 1824−1834.

(2) (a) Ziessel, R.; Grosshenny, V.; Hissler, M.; Stroh, C. *Inorg. Chem.* **2004**, *43*, 4262−4271. (b) Roche, S.; Haslam, C.; Heath, S. L.; Thomas, J. A. *Chem. Commun.* **1998**, *16*, 1681−1682. (c) Tony, K. J. *React. Kinet. Catal. Lett.* **1997**, *60*, 145−155. (d) Kohichi, K. *Organometallics* **1997**, *16*, 2233−2336. (e) Sens, C.; Rodríguez, M.; Romero, I.; Llobet, A.; Parella, T.; Sullivan, B. P.; Benet-Buchholz, J. *Inorg. Chem.* **2003**, *42*, 2040−2048. (f) Khenkin, A. M.; Shimon, L. J. W.; Neumann, R. *Inorg. Chem.* **2003**, *42*, 3331−3339. (g) Gonsalvi, L.; Arends, I. W. C. E.; Sheldon, R. A. *Chem. Commun.* **2002**, *3*, 202−203. (h) Huynh, M. H. V.; Witham, L. M.; Lasker, J. M.; Wetzler, M.; Mort, B.; Jameson, D. L.; White, P. S.; Takeuchi, K. J. *J. Am. Chem. Soc.* **2003**, *125*, 308−309. (i) Riley, D. P.; Shumate, R. F. *J. Am. Chem. Soc.* **1984**, *106*, 3179−3184.

(3) (a) Khan, M. M. T.; Mohiuddin, R.; Vancheesan, S.; Swamy, B. *Ind. J. Chem., Sect. A: Inorg. Bioinorg., Phys., Theor. Anal. Chem.* **1981**, *20A*, 56. (b) Genet, J. P. *Acc. Chem. Res.* **2003**, *36*, 908−918. (c) Serrano, I.; Llobet, A.; Rodríguez, M.; Romero, I.; Benet-Buchholz, J.; Parella, T.; Campelo, J.; Luna, D.; Marinas, J. *Inorg. Chem.* **2006**, *45* (6), 2644−2651.

(4) (a) Takahashi, K.; Yamashita, M.; Ichihara, T.; Nakano, K.; Nozaki, K. *Angew. Chem., Int. Ed.* **2010**, *49*, 4488−4490. (b) Zakzeski, J.; Lee, H.; Leung, Y. L.; Bell, A. T. *Appl. Catal., A* **2010**, *374*, 201−212. (c) Fachinetti, G.; Funaioli, T.; Marchetti, F. *Chem. Commun.* **2005**, *23*, 2912−2914.

(5) (a) Kelly, S. O.; Barton, J. K. *Science* **1999**, *238*, 375. (b) Hall, D. B.; Holmlin, R. E.; Barton, J. K. *Nature* **1996**, *384*, 731. (c) Burrows, C. J.; Muller, J. G. *Chem. Rev.* **1998**, *98*, 1109. (d) Weatherly, S. C.; Yang, I. V.; Thorp, H. H. *J. Am. Chem. Soc.* **2001**, *123*, 1236. (e) Arbuse, A.; Font, M.; Martinez, M. A.; Fontrodona, X.; Prieto, M. J.; Moreno, M.; Sala, X.; Llobet, A. *Inorg. Chem.* **2009**, *48*, 11098−11107.

(6) (a) Sartorel, A.; Miró, P.; Salvadori, E.; Romain, S.; Carraro, M.; Scorrano, G.; Di Valentin, M.; Llobet, A.; Bo, C.; Bonchio, M. *J. Am. Chem. Soc.* **2009**, *131*, 16051−16053. (b) Romain, S.; Bozoglian, F.; Sala, X.; Llobet, A. *J. Am. Chem. Soc.* **2009**, *131*, 2768−2769. (c) Mola, J.; Mas-Marza, E.; Sala, X.; Romero, I.; Rodríguez, M.; Viñas, C.; Parella, T.; Llobet, A. *Angew. Chem., Int. Ed.* **2008**, *47*, 5830−5832.

(7) Tseng, H.; Zong, R.; Muckerman, J. T.; Thummel, R. *Inorg. Chem.* **2008**, *47*, 11763−11773.

(8) Wasylenko, D. J.; Ganesamoorthy, C.; Koivisto, B. D.; Henderson, M. A.; Berlinguette, C. P. *Inorg. Chem.* **2010**, *49*, 2202−2209.

(9) (a) Yamada, H.; Koike, T.; Hurst, J. K. *J. Am. Chem. Soc.* **2001**, *123*, 12775−12780. (b) Collins, M. J.; Ray, K.; Que, L. *Inorg. Chem.* **2006**, *45*, 8009. (c) Bozoglian, F.; Romain, S.; Ertem, M. Z.; Todorova, T. K.; Sens, C.; Mola, J.; Rodríguez, M.; Romero, I.; Benet-Buchholz, J.; Fontrodona, X.; Cramer, C. J.; Gagliardi, L.; Llobet, A. *J. Am. Chem. Soc.* **2009**, *131*, 15176−15187.

(10) Planas, N.; Christian, G. J.; Mas-Marzá, E.; Sala, X.; Fontrodona, X.; Maseras, F.; Llobet, A. *Chem.—Eur. J.* **2010**, *16*, 7965−7968.

(11) (a) Casabo, J.; Pons, J.; Siddiqi, K. S.; Teixidor, F.; Molins, E.; Miravitlles, C. J. *J. Chem. Soc., Dalton Trans.* **1989**, 1401−1403. (b) Levine, R.; Sneed, J. K. *J. Am. Chem. Soc.* **1951**, *73*, 5614−5616.

(12) (a) Gagne, R. R.; Marritt, W. A.; Marks, D. N.; Siegl, W. O. *Inorg. Chem.* **1981**, *20*, 3260. (b) Marks, D. N.; Siegl, W. O.; Gagne, R. R. *Inorg. Chem.* **1982**, *21*, 3140.

(13) Sens, C.; Romero, I.; Rodriguez, M.; Llobet, A.; Parella, T.; Benet-Buchholz, J. *J. Am. Chem. Soc.* **2004**, *126*, 7798−7799.

(14) *Specfit* is a trademark of Spectrum Software Associates.

(15) Data collection with: *APEX II*, versions v1.0-22, v2009.1-0, and v2009.1-02;. Bruker AXS Inc.: Madison, WI, 2007.

(16) Data reduction with: *SAINT*, versions V2.10, V0.60A, and V7.60A; Bruker AXS Inc.: Madison, WI, 2003 and 2007.

(17) *SADABS*, V.2.10, V2008, and V2008/1; Bruker AXS Inc.: Madison, WI, 2003 and 2001. Blessing, J. *Acta Crystallogr.* **1995**, *A51*, 33−38.

(18) *TWINABS*, version 2008/4: Blessing, J. *Acta Crystallogr.* **1995**, *A51*, 33−38.

(19) *SHELXTL*, versions V6.12 and 6.14: Sheldrick, G. M. *Acta Crystallogr.* **2008**, *A64*, 112−122.

(20) Frisch, M. J.; Trucks, G. W.; Schlegel, H. B.; Scuseria, G. E.; Robb, M. A.; Cheeseman, J. R.; Montgomery, J. A., Jr.; Vreven, T.; Kudin, K. N.; Burant, J. C.; Millam, J. M.; Iyengar, S. S.; Tomasi, J.; Barone, V.; Mennucci, B.; Cossi, M.; Scalmani, G.; Rega, N.; Petersson, G. A.; Nakatsuji, H.; Hada, M.; Ehara, M.; Toyota, K.; Fukuda, R.; Hasegawa, J.; Ishida, M.; Nakajima, T.; Honda, Y.; Kitao, O.; Nakai, H.; Klene, M.; Li, X.; Knox, J. E.; Hratchian, H. P.; Cross, J. B.; Bakken, V.; Adamo, C.; Jaramillo, J.; Gomperts, R.; Stratmann, R. E.; Yazyev, O.; Austin, A. J.; Cammi, R.; Pomelli, C.; Ochterski, J. W.; Ayala, P. Y.; Morokuma, K.; Voth, G. A.; Salvador, P.; Dannenberg, J. J.; Zakrzewski, V. G.; Dapprich, S.; Daniels, A. D.; Strain, M. C.; Farkas, O.; Malick, D. K.; Rabuck, A. D.; Raghavachari, K.; Foresman, J. B.; Ortiz, J. V.; Cui, Q.; Baboul, A. G.; Clifford, S.; Cioslowski, J.; Stefanov, B. B.; Liu, G.; Liashenko, A.; Piskorz, P.; Komaromi, I.; Martin, R. L.; Fox, D. J.; Keith, T.; Al-Laham, M. A.; Peng, C. Y.; Nanayakkara, A.; Challacombe, M.; Gill, P. M. W.; Johnson, B.; Chen, W.; Wong, M. W.; Gonzalez, C.; and Pople, J. A. *Gaussian03*, revision C.02; Gaussian, Inc.: Wallingford, CT, 2004.

(21) Dapprich, S.; Komaromi, I.; Byun, K. S.; Morokuma, K.; Frisch, M. J. *THEOCHEM* **1999**, *461−462*, 1−21.

(22) Svensson, M.; Humbel, S.; Froese, R. D. J.; Matsubara, T.; Sieber, S.; Morokuma, K. J. *Phys. Chem.* **1996**, *100*, 19357−19363.

(23) Becke, A. D. *J. Chem. Phys.* **1993**, *98*, 5648.

(24) (a) Lee, C. T.; Yang, W. T.; Parr, R. G. *Phys. Rev. B* **1988**, *37*, 785−789. (b) Rappe, A. K.; Casewit, C. J.; Colwell, K. S.; Goddard, W. A.; Skiff, W. M. *J. Am. Chem. Soc.* **1992**, *114*, 10024−10035.

(25) Andrae, D.; Häußermann, U.; Dolg, M.; Stoll, H.; Preuß, H. *Theor. Chim. Acta* **1990**, *77*, 123−141.
(26) Hehre, W. J.; Ditchfield, R.; Pople, J. A. *J. Chem. Phys.* **1972**, *56*, 2257−2261.
(27) Michelle, M. F.; William, J. P.; Warren, J. H.; Binkley, J. S.; Mark, S. G.; Douglas, J. D.; John, A. P. *J. Chem. Phys.* **1982**, *77*, 3654−3665.
(28) Harvey, J. N. *Faraday Discuss.* **2010**, *145*, 487−505.
(29) Lau, J. K.-C.; Deubel, D. V. *J. Chem. Theory Comput.* **2006**, *2*, 103−106.
(30) Miertus, S.; Scrocco, E.; Tomasi, J. *J. Chem. Phys.* **1981**, *55*, 117−129.
(31) Neese, F. *ORCA—an ab initio, Density Functional and Semiempirical Program Package*, 2.7th ed.; Universität Bonn: Bonn, Germany, 2009.
(32) (a) Grimme, S. J. *Comput. Chem.* **2004**, *25*, 1463−1473. (b) Grimme, S. J. *Comput. Chem.* **2006**, *27*, 1787−1799.
(33) (a) Schafer, A.; Horn, H.; Ahlrichs, R. *J. Chem. Phys.* **1992**, *97*, 2571−2577. (b) Schafer, A.; Huber, C.; Ahlrichs, R. *J. Chem. Phys.* **1994**, *100*, 5829−5835.
(34) (a) Laurent, F.; Plantalech, E.; Donnadieu, B.; Jimenez, A.; Hernandez, F.; Martinez-Ripoll, M.; Biner, M.; Llobet, A. *Polyhedron* **1999**, *18*, 3321−3331. (b) Romero, I.; Rodriguez, M.; Llobet, A.; Collomb-Dunand-Sauthier, M. N.; Deronzier, A.; Parella, T.; Soteckli-Evans, H. *J. Chem. Soc., Dalton Trans.* **2000**, 1689−1694. (c) Sala, X.; Plantalech, E.; Poater, A.; Rodriguez, M.; Romero, I.; Sola, M.; Llobet, A.; Jansat, S.; Gomez, M.; Stoeckli-Evans, H.; Benet-Buchholz, J. *Chem.—Eur. J.* **2006**, *12*, 2798−2807. (d) Sens, C.; Rodríguez, M.; Romero, I.; Llobet, A.; Parella, T.; Benet-Buchholz, J. *Inorg. Chem.* **2003**, *42*, 8385−8394. (e) Masllorens, E.; Rodríguez, M.; Romero, I.; Roglans, A.; Parella, T.; Benet-Buchholz, J.; Poyatos, M.; Llobet, A. *J. Am. Chem. Soc.* **2006**, *128* (16), 5306−5307.
(35) (a) Anderson, P. E.; Deacon, G. B.; Haarmann, K. H.; Keene, F. R.; Meyer, T. J.; Reitsma, D. A.; Skelton, B. W.; Strouse, G. F.; Thomas, N. C.; Treadway, T. A.; White, T. A. *Inorg. Chem.* **1995**, *34*, 6145−6157. (b) Barqawi, K. R.; Llobet, A.; Meyer, T. J. *J. Am. Chem. Soc.* **1988**, *110*, 7751−7759. (c) Llobet, A. *Inorg. Chim. Acta* **1994**, *221*, 125−131.
(36) Mola, J.; Dinoi, C.; Sala, X.; Rodríguez, M.; Romero, I.; Parella, T.; Fontrodona, X.; Llobet., A. *Dalton Trans.* **2011**, *40*, 3640−3646.
(37) Allen, L. R.; Craft, P. P.; Durham, B.; Walsh, J. *Inorg. Chem.* **1987**, *26*, 53−56.
(38) (a) Rapaport, I.; Helm, L.; Merbach, A. E.; Bernhard, P.; Ludi, A. *Inorg. Chem.* **1988**, *27*, 873−879. (b) Leising, R. A.; Ohman, J. S.; Takeuchi, K. J. *Inorg. Chem.* **1988**, *27*, 3804−3809. (c) Arce Sagues, J. A.; Gillard, R. D.; Williams, P. A. *Transition Met. Chem.* **1989**, *14*, 110. (d) Sala, X.; Romero, I.; Rodriguez, M.; Llobet, A.; Gonzalez, G.; Martinez, M.; Benet-Buchholz, J. *Inorg. Chem.* **2004**, *43*, 5403−5409.
(39) (a) Liu, Y.; Turner, D, B.; Singh, T. N.; Angeles-Boza, A. M.; Chouai, A.; Dunbar, K. R.; Turro, C. *J. Am. Chem. Soc.* **2009**, *131*, 26−27. (b) Gabrielsson, A.; Zalis, S.; Matousek, P.; Towrie, M.; Vlcek, A. *Inorg. Chem.* **2004**, *43*, 7380−7388. (c) Marciniec, B.; Pietraszuk, C. *Organometallics* **1997**, *16*, 4320−4326.